Exploring New Targeted Therapies for Sonic Hedgehog (SHH) Medulloblastoma

By

Stephanie Borlase

A Thesis submitted to the Faculty of Graduate Studies of

The University of Manitoba

In partial fulfilment of the requirements of the degree of

MASTER OF SCIENCE

Department of Biochemistry and Medical Genetics

University of Manitoba

Winnipeg

Abstract

Medulloblastoma (MB) is the most common malignant primary pediatric brain tumor and is currently divided into 4 molecular subgroups that exhibit different genomic alterations, gene expression profiles and response to treatment. We have previously shown a novel role for the MEK/MAPK pathway in specifically contributing to Sonic Hedgehog (SHH) MB tumor progression. Here, we compared the effect of the MEK inhibitor (MEKi) selumetinib to the more potent MEKi trametinib on tumor cell properties *in vitro* and assessed the effect of trametinib in 3 orthotopic MB xenograft models *in vivo*. Trametinib significantly reduced tumorsphere size, stem/progenitor cell proliferation and viability at much lower concentrations than selumetinib. RNA sequencing corroborated these findings with significant decreases in cell cycle and stem cell pathways concomitant with increases in pathways associated with cell differentiation and ciliopathies following MEKi treatment. Importantly, trametinib also decreased tumor growth and increased survival *in vivo* and this was accompanied by similar decreases in cell cycle related pathways as well as increases in IL6/JAK STAT3 signaling. Our study reveals a novel role for trametinib in effectively attenuating MB tumor progression and warrants further investigation of this potent MEK1/2 inhibitor either alone or in combination with other targeted therapies for the treatment of SHH MB.

Keywords: SHH medulloblastoma, trametinib, xenografts, RNA sequencing, tumorspheres

Acknowledgments

I would like to thank my amazing supervisor Dr. Tamra Werbowetski-Ogilvie for her unconditional help and support, knowledge, guidance, direction, and mentorship throughout my Master of Science. I am so grateful that I was able to join Dr. Ogilvie's lab where I learned new techniques, received multiple studentships and awards, and obtained 2 first author publications as well as multiple co-authored papers. I would like to especially thank Dr. Ogilvie for supporting my PhD goals and for providing me with the help and assistance to reach these goals.

I would like to thank my committee members Dr. Tamra Werbowetski-Ogilvie, Dr. Britt Drögemöller, and Dr. Brad Doble for their support and assistance throughout my thesis. They provided their valuable time to attend my fall review meetings, annual FGS review meetings, and thesis proposal meeting. Their valuable feedback, constructive criticism and guidance helped increase my knowledge and better prepare me for my PhD. I would like to additionally thank Dr. Doble for his support with my University of Toronto PhD applications as well as a University of Toronto studentship.

Thank you to my lab members Dr. Jamie Zagozewski, Ludivine Morrison and Dr. Victor Gordon for teaching me new laboratory techniques and for always being available to provide assistance, guidance and answer any questions I had. I would like to especially thank Lu for her help with my numerous animal studies and for the immunohistochemistry, mouse brain dissociations and migration assays she completed for me.

I thank Agnes Fresnoza and Dr. Mike Jackson for their help with my animal studies. I am extremely grateful and thankful for the funding that I received from the Rady Faculty of Health Sciences Studentship and Research Manitoba-University of Manitoba WM Ross Scholarship-CancerCare Manitoba Foundation Master's Studentship Award.

List of Tables

List of Figures

Abbreviations

Medulloblastoma (MB), Sonic Hedgehog (SHH), MEK inhibitor (MEKi), cerebrospinal fluid (CSF), Catenin Beta 1 (*CTNNB1*), large cell and anaplastic (LCA), MB with extensive nodularity (MBEN), cancer stem cell (CSC), granule neuron progenitor cell (GNPC), Orthodenticle Homeobox 2 (*OTX2*), Patched (*PTCH1*), suppressor of fused (*SUFU*), smoothened (*SMO*), glioma-associated oncogene (*GLI1*), external granular layer (EGL), tumor protein 53 (*TP53*) telomerase reverse transcriptase (*TERT*), nonobese diabetic severe combined immune deficiency (NOD SCID), nonobese diabetic severe combined immune deficiency gamma (NSG), patient derived xenograft (PDX), blood-brain-tumor barrier (BBTB), gene set enrichment analysis (GSEA), RNA sequencing (RNA-seq), immunohistochemistry (IHC), formalin-fixed paraffin-embedded (FFPE), food and drug administration (FDA)

Contributions

Stephanie Borlase and Dr. Tamra Werbowetski-Ogilvie are responsible for conception and design of experiments, assembly, and interpretation of data. Stephanie Borlase is responsible for completing the majority of the experiments, data collection and writing the thesis. Ludivine Morrison completed the immunohistochemistry and mouse brain dissociations. Agnes Fresnoza performed the animal surgeries and Dr. Mike Jackson performed the mice MRI.

Chapter I: Introduction

Medulloblastoma

Brain tumors are among the most prevalent forms of childhood cancer and account for nearly 20% of all pediatric cancer diagnoses[1]. They also constitute the highest number of cancer-related deaths in both Canadian and American children under 14 years old[1]. Medulloblastoma (MB) is the most common malignant primary pediatric brain tumor and is highly heterogeneous[2]. Primary MB tumors typically develop in the cerebellum and along the fourth ventricle resulting in obstructive hydrocephalus[3,4]. However, frequent dissemination through the cerebrospinal fluid (CSF) drives metastasis and tumor recurrence[5]. MB patients generally exhibit a short duration of symptomatology due to the rapid growth of MB tumors that can range from 1 to 3 months prior to presentation[6,7]. The current treatment consists of aggressive surgery, high doses of cytotoxic chemotherapy and/or radiation to the whole brain and spinal cord. Over the last 2 decades, risk-stratification and treatment regimens have been defined based on the presence of metastasis, extent of resection at diagnoses and the age of the patient[4,8]. Based on these criteria, patients are stratified into one of three different treatment groups. The first group consists of patients older than 3 years of age with standard risk disease. These children and adults receive total or near total resection of their tumors and have no evidence of tumor cells in their CSF[8,9]. The second treatment group consists of patients older than 3 years of age with high-risk disease. This is defined based on the presence of a residual tumor following surgery that is greater than 1.5 cm^2 or by the presence of metastasis[4]. Patients in this second treatment group with high-risk disease have increased risk of tumor recurrence or death compared to the first treatment group with average risk disease[8]. Finally, patients younger than 3 years of age make up the last treatment group. Radiation therapy is typically used for MB patients over 3 years of age. However, radiation is not recommended for

children and infants under 3 years old[4]. This third treatment group typically receives high dose chemotherapy to hopefully delay or completely remove the need for radiation therapy thus allowing the nervous system to further develop in these young patients[10]. Despite improved clinical outcomes, 40% of patients succumb to their disease while survivors are left with extensive cognitive and physical delays following surgery and treatment[11].

Medulloblastoma Histological Classification

The 2007 edition of the WHO Classification of Tumors of the Central Nervous System utilized histological criteria to stratify MB into different subgroups[12]. MB tumors are also known as blue cell tumors because they present as small, round, blue cells under the microscope[4]. This is attributed to the presence of large nuclei surrounded by minimal cytoplasm in less differentiated cells when stained with hematoxylin and eosin (H&E)[13]. MB can be divided into four main histological classes that are known as classic, large cell and anaplastic (LCA), desmoplastic and nodular and MB with extensive nodularity (**Fig. 1**)[4,14].

Classic Histology

Classic histology is the most common MB tumor variant and accounts for 72% of all MB tumors. Classic histology is characterized by the presence of small, round, undifferentiated cells with a high nuclear to cytoplasmic ratio and hyperchromatic nuclei (**Fig. 1A**) which means that the nucleus looks darker than usual when viewed under a microscope[4]. Approximately 40% of all classic MB tumors exhibit Homer-Wright rosettes which present as arrangements of differentiated tumor cell groups around a central region that contains neuropil[14]. There is a strong relationship

between Catenin Beta 1 (*CTNNB1)* mutations and nuclear accumulation of β-catenin which is indicative of WNT pathway activation in classic MB[15]. The majority of WNT tumors therefore present with classic histology, and this nuclear accumulation of β-catenin is associated with positive clinical outcomes in this subgroup[15,16].

Large Cell and Anaplastic Histology

The large cell and anaplastic (LCA) variant is the most malignant histologic subtype and is characterized by nuclear pleiomorphism with large nuclei, prominent nucleoli and abundant cytoplasm (**Fig. 1B**)[14,17]. The combination of large cell and anaplastic histology accounts for approximately 10% of all MB tumors[4]. A typical feature observed in large cell and anaplastic MB tumors is cell-cell wrapping with the engulfed cell often undergoing cell death. Most large cell MB tumors exhibiting large, round neoplastic cells with prominent nucleoli are heterogeneous, as they contain areas with anaplastic and classic tumor cells. Anaplastic MB tumors consist of tumor cells with enlarged pleomorphic nuclei that exhibit variation in size and shape[14,17,18]. The nuclear to cytoplasmic ratio is high and proliferative as well as apoptotic indices are also high compared to those in large cell MB tumors.

Desmoplastic and nodular Histology

Desmoplastic and nodular MB is characterized by nodules of differentiated neurocytic cells that are surrounded by internodular, reticulin-rich zones (**Fig. 1C**)[4]. The internodular zones contain highly proliferative and densely packed cells[14]. This was determined by immunohistochemical staining with proliferative markers demonstrating that the internodular zones are associated with

higher mitotic activity of undifferentiated cells that are present in these areas[14]. Desmoplastic and nodular MB tumors rarely exhibit nuclear accumulation of p53 which may indicate an underlying somatic or germline mutation in *TP53*.

Extensive Nodularity Histology

MB with extensive nodularity (MBEN) is typically seen in infant tumors and is characterized by expanded nodular or lobular architecture with elongated reticulin-free, neuropil-rich zones[19] (**Fig. 1D**). There is normally a 'streaming' pattern observed in these tumors where linear arrays of neurocytic cells connect adjacent nodules. The internodular zones are reduced compared to desmoplastic and nodular MB tumors but they show the same characteristic features of undifferentiated, proliferating tumor cells within a dense reticulin network (**Fig. 1E**)[4].

Figure 1: Medulloblastoma tumor histology

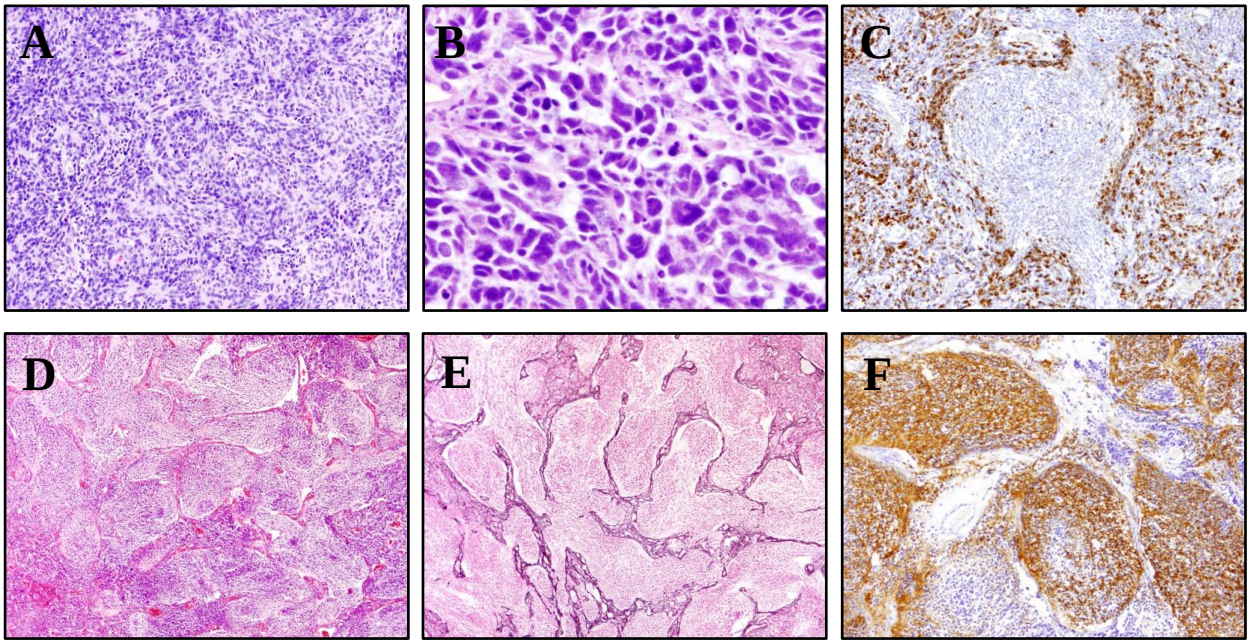

A-F. Medulloblastoma (MB) tumor histology. Classic medulloblastoma (A), large cell/anaplastic MB (B), desmoplastic/nodular MB (C), MB with extensive nodularity (D-F).

Taken from *Primary pediatric brain tumors of the posterior fossa: Part II A comprehensive overview of medulloblastoma*, 2017 *with permission from Springer Nature

Medulloblastoma heterogeneity and the evolution of subgroups

MB is a highly heterogeneous disease that consists of a combination of malignant cells that display distinct genetic, molecular, and cellular characteristics[4]. Extensive heterogeneity exists not only between tumors (intertumoral heterogeneity) but also within tumors (intratumoral heterogeneity)[4]. One of the layers of intratumoral heterogeneity to consider is the cancer stem cell hierarchy. Over the past two decades, the cancer stem cell (CSC) model of tumor progression has been extensively explored. The model was originally intended to explain the cellular and functional heterogeneity found within a variety of malignancies, including MB[4]. CSCs exhibit stem cell like properties which include self-renewal capacity and multi-lineage differentiation[20,21]. This means that a CSC can either divide to generate more identical CSCs, or a CSC can divide into a more differentiated cell type called a progenitor cell. Progenitor cells are highly proliferative, but they have limited self-renewal capacity and therefore cannot maintain the CSC pool or tumor growth long term. Theoretically, only a CSC can give rise to a new tumor following long-term passage *in vitro* or *in vivo*.

In addition to the cellular heterogeneity observed in MB, over a decade of extensive multi-omic sequencing analyses have been completed and have revolutionized molecular classification of these highly aggressive tumors, revealing extensive intertumoral heterogeneity. The current consensus is that MB is divided into at least 4 distinct molecular subgroups (**Table 1**): WNT, Sonic Hedgehog (SHH), Group 3 and Group 4[13,22,23]. These subgroups exhibit different genomic alterations, gene expression profiles, developmental cell of origin and response to treatment. Recently, extensive additional substructure has been defined within each molecular subgroup[2,13,22,23]. This additional stratification has led to the complete restructuring of the different

MB subgroups, which have now been incorporated into the World Health Organization (WHO) Classification of Central Nervous System Tumors[5]. MB is currently subdivided into as many as 14 molecular subtypes underscoring the extensive heterogeneity and complexity between and within the major subgroups[24-26]. This novel molecular classification system can predict patient prognosis and has the potential to drive subgroup or even subtype-specific treatment regimens. Importantly, molecular subgrouping/subtyping has improved risk stratification and has ultimately provided novel opportunities to increase therapy for patients with high-risk tumors and reduce therapy for those with lower-risk tumors[27].

The following sections will discuss each MB subgroup and their corresponding subtypes. The SHH subgroup will be the most extensively discussed, as this is the main focus of my thesis. Genetic and molecular alterations, prognosis, and cell of origin for each subgroup will be described.

Table 1: Medulloblastoma Subgroups

Subgroup	WNT	SHH	Group 3	Group 4
Frequency	10%	30%	25%	35%
Peak age (years old)	3-10 and 10-17	0-3 and 17+	3-10	3-10
Male to female ratio	1:1	2:1	2:1	2:1
Molecular and genetic alterations	WNT signaling *CTNNB1* mutation Monosomy 6	SHH signaling *PTCH1*/*SMO*/ *SUFU*/*GLI* mutation *MYCN* amplification	*MYC* amplification *OTX2* amplification/ overexpression TGF-β signaling	*MYCN* amplification *OTX2* amplification/ overexpression *CDK6* amplification NF-KB signaling Isochromosome 17q
Metastasis	Rare	Uncommon	Very frequent	Frequent
Prognosis	Good	Intermediate	Poor	Intermediate
Putative cell of origin	Mossy fiber neuron lineage from lower rhombic lip	Granule neuron progenitor cells (GNPCs) of the EGL	Undifferentiated stem/progenitor cell from cerebellar glutamatergic lineage	More differentiated neuronal-like cell that shares marker expression with unipolar brush cells

MB is divided into 4 major molecular subgroups that exhibit different genomic alterations, gene expression profiles, response to treatment, and developmental cell of origin. The 4 subgroups are WNT, Sonic Hedgehog (SHH), Group 3 and Group 4.

Adapted from Cavalli et al., *Cancer Cell*, 2017.

The WNT medulloblastoma subgroup

Genetic and Molecular Alterations

WNT tumors represent the most uncommon group of MB with just 10% of diagnoses[4]. WNT tumors are characterized by the up regulation of genes associated with the WNT signaling pathway (**Fig. 2**). The WNT signaling pathway plays an essential role in brain development and is important for regulating self-renewal of neural precursors during neurogenesis[28-30]. In the canonical WNT signaling pathway, ß-catenin (encoded by Catenin Beta 1 (*CTNNB1*)) is the main signaling molecule[31,32]. In the absence of WNT ligands, glycogen synthase kinase 3 (*GSK3*) mediates the phosphorylation of β-catenin, which ultimately triggers its proteolysis[33]. β-catenin levels are therefore kept low in the cytoplasm and transcription is inhibited[31,32]. However, when WNT ligands are present, they bind to frizzled and this inhibits the proteosomal degradation of β-catenin resulting in an accumulation of β-catenin and upregulated transcription of target genes[34,35]. Somatic mutations in downstream WNT signaling pathway genes such as *CTNNB1*, Axis inhibition protein 1 (*AXIN1*) and Adenomatous polyposis coli (*APC*) are the hallmark genetic events that define this subgroup[36-40]. Gibson et al. showed that aberrant WNT signaling in the progenitor cells of the dorsal brainstem leads to development of WNT MB, providing the first evidence for the cell of origin for this subgroup[41]. They showed that WNT subgroup tumors arise from lower rhombic lip progenitor cells of the dorsal brainstem and that mutations in *Ctnnb1* disrupts the normal differentiation and migration of these progenitor cells resulting in abnormal cell accumulation[41]. They also determined that an additional mutation in *TP53* resulted in formation of classic MB that was confined to the dorsal brainstem and displayed expression profiles similar to WNT MB.

Figure 2: Wnt signaling pathway

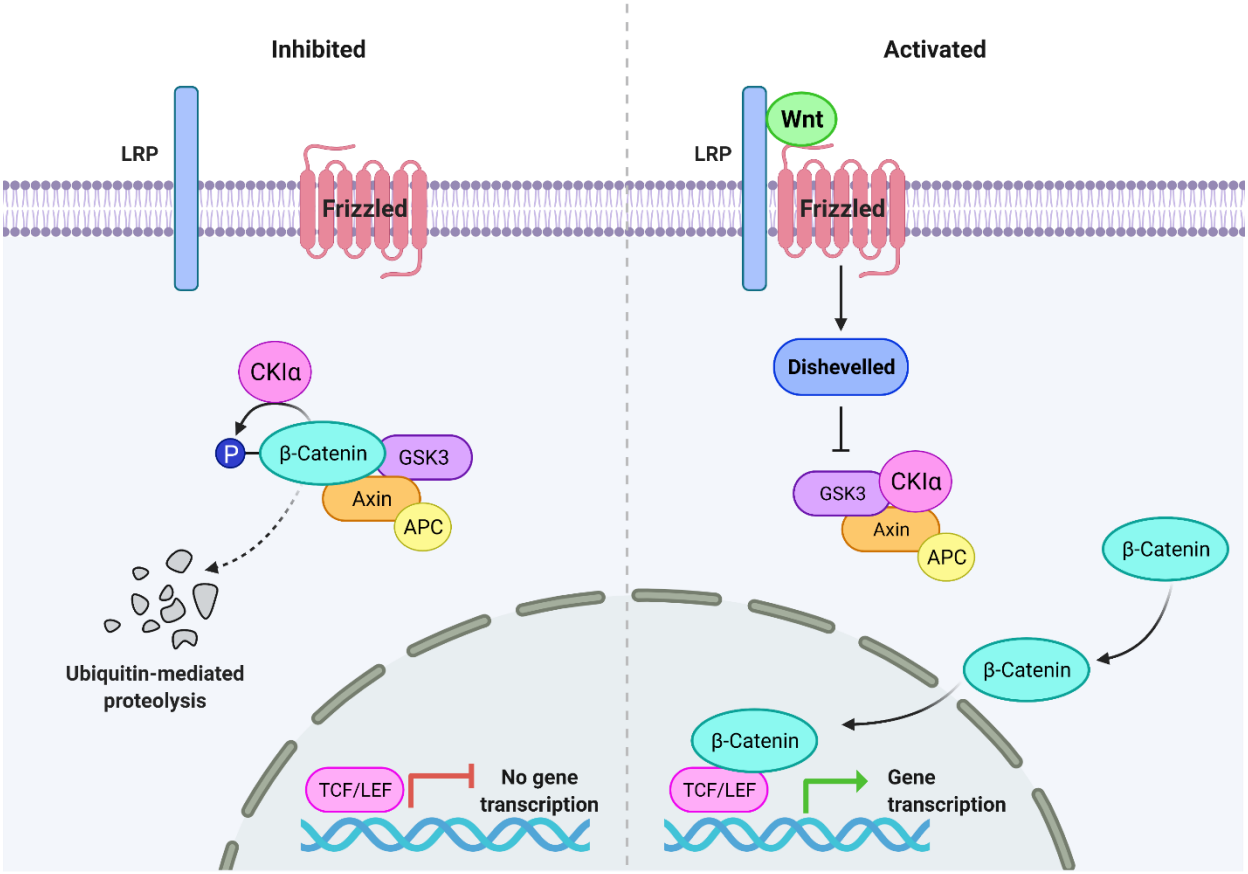

The Wingless (WNT) pathway plays a critical role in WNT-activated MB tumorigenesis. Canonical (β-catenin dependent) WNT signaling plays a key role in the formation of the midbrain/hindbrain boundary through the control of neural stem cell proliferation and is believed to drive tumor initiation in WNT MB. When no WNT is present, β-catenin levels are kept low through phosphorylation-targeted destruction by the multi-protein destruction complex (Axin, APC, GSK3, and CK1α) leading to target gene repression. Binding of WNT to the Frizzled (FZD) receptor and its co-receptor LDL-receptor-related protein 5/6 (LRP) results in elevated intracellular β-catenin through the inhibition of targeted destruction. Stable non-phosphorylated β-catenin is translocated into the nucleus where it displaces Groucho and activates TCF/LEF, enabling transcription of target genes such as cyclin D1 and MYC.

Adapted from *"Wnt Signaling Pathway, Activation and Inhibition",* BioRender.com (2021).

Demographics and Prognosis

WNT tumors have the most favorable prognosis of the 4 subgroups as they rarely metastasize and have a 5-year survival rate of 95% or better[2,13]. This could be attributed to the fact that WNT MBs have been shown to exhibit a highly aberrant and leaky vasculature, which allows substantial accumulation of intra-tumoral chemotherapy[42] and is likely contributing to their more robust clinical response. Therefore, patients with WNT MB normally receive the standard current treatment, which includes surgery, chemotherapy, and radiation. Recently, it has been suggested that patients with WNT tumors that have not metastasized should receive reduced chemotherapy and radiation[43]. However, Nobre et al[44]. have shown that maintenance chemotherapy in WNT tumors is a strong predictor of tumor resistance and relapse and that individuals treated with high doses of chemotherapy had significantly improved clinical outcomes. Additionally, targeted therapies that inhibit the WNT signaling pathway have been used in combination with other signaling pathway antagonists. For example, the WNT and PIK/AKT signaling pathways have been shown to exhibit crosstalk. As such, PI3K/AKT inhibitors have been used to target the WNT pathway[45]. Baryawno et al.[46] have shown that the PI3K/AKT inhibitor, OSU03012 downregulates WNT signaling by activating GSK3, which results in the degradation of β-catenin.

WNT Subtypes

Recently, the WNT subgroup has been further subdivided into two molecular subtypes: WNT-α and WNT-β (**Table 2**)[4]. These subtypes differ in the age at diagnosis, with WNT-α tumors having a median age of 10 years old, and WNT-β tumors having a median age of 20 years old[24].

Table 2: The WNT medulloblastoma subtypes

Subgroup		**WNT**	
Subtype		**WNTα**	**WNTβ**
Demographics	Frequency (%)	65	35
	Age (years old)	Median age of 10	Median age of 20
	% male : % female	45% male : 55% female	
Clinical features	Histology	Classic	
	Metastases	9%	21%
	Survival	97%	100%
Molecular features	Driver events Cytogenetics	- *CTNNB1*, *DDX3X* or *SMARCA4* mutations - Monosomy 6	

The Wingless (WNT) subgroup is divided into 2 different subtypes, WNTα and WNTβ based on demographics, and clinical and molecular features.

Adapted from Hovestadt et al. *Nature Reviews Cancer,* 2019 and Cavalli et al., *Cancer Cell*, 2017.

Group 3 and Group 4 medulloblastoma subgroups

Demographics and Prognosis

Group 3 and Group 4 MB are also known as the "non-SHH/WNT" subgroups, and both share similar clinical presentations and molecular characteristics. Group 3 makes up 25-30% of MB diagnoses and Group 4 is the most common MB subgroup with 35% of diagnoses[47]. However, less is known about the molecular mechanisms that drive these two subgroups compared to WNT and SHH[13]. In contrast to the WNT subgroup, Group 3 MB tumors have a very high rate of metastasis which is a major contributor to their poor prognosis[4]. Group 3 patients have the worst prognosis of the 4 subgroups with infants having a 5-year OS of 45% and children displaying a 5-year OS of 58%[47] while Group 4 MB tumors have an intermediate prognosis[13].

Group 3 and Group 4 Cell of Origin

Relatively little is known about the cell of origin for Group 3 and Group 4 tumors. It has been suggested that Group 3 tumors may arise from a neural stem cell or a de-differentiated granule neuron progenitor cell (GNPC) and that Group 4 tumors arise from progenitor cells of the upper rhombic lip. Kawauchi et al.[48] and Pei et al.[49] showed that Group 3 tumors exhibit significant similarities to embryonic stem cells, neural stem cells, and induced pluripotent stem cells, suggesting that these tumors predominantly consist of undifferentiated, more primitive cell types[48-50]. Lin et al.[51] have shown that deep cerebellar nuclei or their earlier precursors from the upper rhombic lip are the putative cell of origin for Group 4 tumors. Hovestadt et al.[52] also analyzed Group 4 MB tumors using single-cell transcriptomes and determined that these tumors consist almost exclusively of more differentiated neuronal-like cells and resembled the unipolar brush cell

lineage of the cerebellum which is a glutamatergic neuronal cell population derived from the upper rhombic lip.

Genetic and Molecular Alterations

Group 3 is most often associated with amplification and overexpression of the MYC proto-oncogene (*MYC*) while Group 4 tumors are associated with the MYCN proto-oncogene (*MYCN*) amplification[13,53]. It has also recently been shown that Orthodenticle Homeobox 2 (*OTX2*) regulates MB stem-cell function in a subgroup-dependent manner[54,55]. In fact, our lab has shown that *OTX2* plays an inhibitory role when overexpressed in SHH MB but is oncogenic in Group 3 and 4 MB. OXT2 is a transcription factor that regulates normal cerebellar development[54]. OTX2 has previously been shown to be oncogenic in a number of different cancers and recent studies have revealed that OTX2 is overexpressed in Group 3 and Group 4 MB and is a key driver of tumorigenesis in these MB subgroups[56]. OTX2 promotes tumor cell growth and self-renewal while inhibiting cell differentiation *in vitro*. OTX2 also increases tumor initiation from MB stem and progenitor cells *in vivo*[54,55]. Recent work by our lab[55] has also characterized the OTX2 regulatory network and identified novel relationships between OTX2 and genes associated with neuronal differentiation and axon guidance signaling in Group 3 and Group 4 MB stem/progenitor cells. These findings suggest that OTX2 actively represses differentiation while maintaining Group 3 and Group 4 MB cells in a primitive, stem/progenitor cell state. Additionally, we also recently identified an OTX2 regulatory network that controls the balance between the Group 3 MB stem cell state and differentiation[57]. OTX2 broadly restricts expression of transcription factors that are critical for neuronal differentiation, including members of the Paired box (PAX) gene family such as PAX3. In addition, Mechanistic Target of Rapamycin Kinase (mTORC1) signaling was

identified as a downstream effector of OTX2-PAX3, revealing a novel role for protein synthesis pathways in Group 3 MB tumor progression[57].

Treatment of Group 3 and Group 4 MB

Group 3 MB metastasize frequently and are the most aggressive subgroup making these tumors very hard to treat with the standard of care options[4]. There is a critical need to identify pathways contributing to Group 3 MB tumor progression to develop targeted therapies that can reduce toxicity and improve survival in these young patients. *MYC* amplification provides a target for Group 3 MB treatment. In fact, Morfouace et al.[58] have identified two FDA approved drugs named pemetrexed and gemcitabine that preferentially inhibit proliferation of Group 3 tumors that exhibit *MYC* amplification or overexpression. Pemetrexed is a folate pathway inhibitor that directly targets phosphoribosyl glycinamide formyltransferase (GART), dihydrofolate reductase (DHFR) and thymidylate synthase (TS) and gemcitabine is a DNA and RNA synthesis inhibitor that blocks DNA replication and deoxynucleotide triphosphate (dNTP) synthesis[58]. Both drugs displayed high selectivity and a diverse mechanism of action. Together, the combination of these two drugs resulted in increased survival in a Group 3 mouse xenograft model[58]. Additionally, OTX2 and its downstream effector molecules also serve as potential therapeutic targets for these aggressive subgroups as OTX2 is amplified or overexpressed in both Group 3 and Group 4 tumors. There is currently no treatment that specifically targets OTX2, but studies have shown that the use of retinoic acid can reduce OTX2 expression and induce neuronal differentiation[59]. Unfortunately, this treatment option ultimately results in relapse as the tumor cells quickly become resistant to retinoic acid[60,61].

Group 3 and Group 4 Subtypes

Group 3 and Group 4 have recently been further subdivided into 8 different subtypes designated as I, II, III, IV, V, VI, VII and VIII (**Table 3 and 4**)[2,26]. Subtype I tumors consist of a mix of Group 3 and Group 4 tumors and is the least common subtype. These tumors are enriched for amplification of the orthodenticle homeobox 2 (*OTX2*) oncogene and activation of growth factor independent 1 (*GFI1*) or *GFI1B*[2,26]. Subtypes II, III and IV represent Group 3 tumors with subtypes II and III having *MYC* amplification which is associated with poor prognosis[2,26]. Group 4 MBs mostly make up Subtypes V, VI and VII with subtype V exhibiting amplification of both *MYC* and *MYCN*[2,26]. Subtype VIII is purely Group 4 and is the most common of the 8 subtypes.

Table 3: The Group 3 medulloblastoma subtypes

Subgroup		**Group 3**			
Subtype		I	II	III	IV
Demographics	Frequency (%)	4	13	9	10
	Age (years old)	3-10	3-10	3-10	0-3 and 3-10
	% male : % female)	60% : 40%	77% : 23%	78% : 22%	68% : 32%
Clinical features	Histology	Classic > desmoplastic	LCA, classic	Classic > LCA	Classic
	Metastases	35	57	56	58
	Survival	70	50	43	80
Molecular features	Driver events	*GFI1* and *GFI1B* activation *OTX2* amplification	*MYC* amplification *GFI1* and *GFI1B* activation *KBTBD4*, *SMARCA4*, *CTDNEP1* or *KMT2D* mutation	*MYC* amplification (less)	No common driver events

The Group 3 and Group 4 MB subgroups are currently divided into 8 different subtypes based on demographics, clinical and molecular features; Subtypes I, II, III, IV, V, VI, VII and VIII.

Adapted from Hovestadt et al. *Nature Reviews Cancer,* 2019

Table 4: The Group 4 medulloblastoma subtypes

Subgroup		**Group 4**			
Subtype		V	VI	VII	VIII
Demographics	Frequency (%)	8	9	22	25
	Age (years old)	3-10	3-10	3-10	3-10 and 10-17
	% male : % female)	71% : 29%	67% : 33%	66% : 34%	75% : 25%
Clinical features	Histology	Classic	Classic	Classic	Classic
	Metastases	62	45	45	50
	Survival	59	81	85	81
Molecular features	Driver events	*MYC* or *MYCN* amplification	*PRDM6* activation *MYCN* amplification (less)	*KBTBD4* mutation	*PRDM6* activation *KDM6A*, *ZMYM3* or *KMT2C* mutation

The Group 3 and Group 4 MB subgroups are currently divided into 8 different subtypes based on demographics, clinical and molecular features; Subtypes I, II, III, IV, V, VI, VII and VIII.

Adapted from Hovestadt et al. *Nature Reviews Cancer,* 2019

The SHH medulloblastoma subgroup

Genetic and molecular alterations

SHH MB is characterized by activation of the SHH signaling pathway (**Fig. 3**) and is comprised of very high-risk groups of both children and infants that exhibit significant intertumoral heterogeneity. This accounts for the majority of treatment failures despite aggressive therapy[8,24,25,62-65]. Mutations in the SHH signaling pathway represent the most common genetic events observed in these tumors, including inactivating germline or somatic mutations and deletions of Patched (*PTCH1)* and of suppressor of fused homologue (*SUFU*) as well as activating mutations in smoothened homologue (*SMO*) and amplifications of glioma-associated oncogene (*GLI1* and *GLI2*)[26,66]. Germline mutations of the SHH inhibitor *SUFU* predispose individuals to MB. Additionally, other genomic abnormalities can also cause SHH MB. The *PTCH* gene is located on chromosome 9q and deletion of this chromosome is limited to SHH MB[4]. Chromosome 9q deletion is the most common chromosomal abnormality found in this subgroup[23,47,67]. The link between MB and the SHH signaling pathway was originally made through studies of individuals with Gorlin syndrome[4]. Gorlin syndrome is a disease that results from mutations in the SHH receptor *PTCH.* Gorlin syndrome is characterized by macrocephaly, skeletal abnormalities and in some patients, a high rate of cancer, including SHH MB[4,13,68].

The SHH signaling pathway plays a crucial role in the control of GNPC proliferation in the external granular layer (EGL) of the cerebellum, as well as in glial differentiation in the cerebellar cortex[69-71] and is believed to drive tumor pathogenesis in the SHH MB subgroup[13]. When the SHH ligand is not present, the membrane bound receptor PTCH plays an inhibitory role

that represses SHH signaling[72]. However, when the SHH ligand is present, it binds to the PTCH receptor which releases its inhibitory effect on SMO, a member of the G protein-coupled receptor family[73]. Release of SMO results in the activation of the zinc-finger proteins of the glioma associated oncogene transcription factor family including GLI1, GLI2 and GLI3[72]. GLI proteins can function as either transcription activators or repressors. When the SHH ligand is not present, GLI2 and GLI3 are phosphorylated by protein kinase A (PKA), glycogen synthase kinase 3 (GSK3), and casein kinase 1 (CK1) which results in their proteolytic cleavage generating the repressor forms (GLIr)[72]. When SMO is activated, transcriptionally active forms of GLI (GLIa) are formed in combination with inhibition of suppressor of fused (SUFU), a protein responsible for sequestering GLI in the cytoplasm[72,74]. The activating forms of GLI then translocate to the nucleus where they replace the repressor forms of GLI on target genes resulting in transcriptional activation[74].

Many studies have demonstrated that primary cilia are essential for SHH signaling during normal human development and that mutations in ciliary genes can lead to aberrant SHH signaling and disorders called ciliopathies[75,76]. Han et al.[75] have shown that both the primary cilium and SHH signaling are required for GNPC proliferation in the external granular layer of the cerebellum. Moreover, Aguilar et al.[77] have shown that ciliary conditional mutant mice have a hypoplastic cerebellar vermis in which the proliferation of GNPCs in the cerebellum is severely reduced in response to SHH signaling. In addition, Han et al.[75] demonstrated that SHH MB tumorigenesis occurred when a mutation upstream of the primary cilia was present such as *PTCH1* or *SMO*. In contrast, when a downstream protein target was mutated such as *GLI*, removal of cilia was required for tumor growth. They therefore determined that primary cilia are either required for MB tumor

growth or can inhibit MB tumor formation depending on the underlying oncogenic event. Additionally, they found that the presence or absence of cilia was associated with specific MB subgroups. For example, primary cilia were found in WNT and SHH MB tumors but not in Group 3 or Group 4 MB suggesting that SHH MB may result from mutations upstream of the primary cilia such as *PTCH1* or *SMO* and will only grow from a downstream mutation such as *GLI* when cilia are not present. Together these data suggest that primary cilia are crucial for SHH signaling and GNPC proliferation. Defects in ciliary genes lead to aberrant SHH signaling which affect GNPC proliferation in the cerebellum resulting in severe cerebellar defects or SHH MB.

Figure 3: Sonic Hedgehog (SHH) signaling pathway

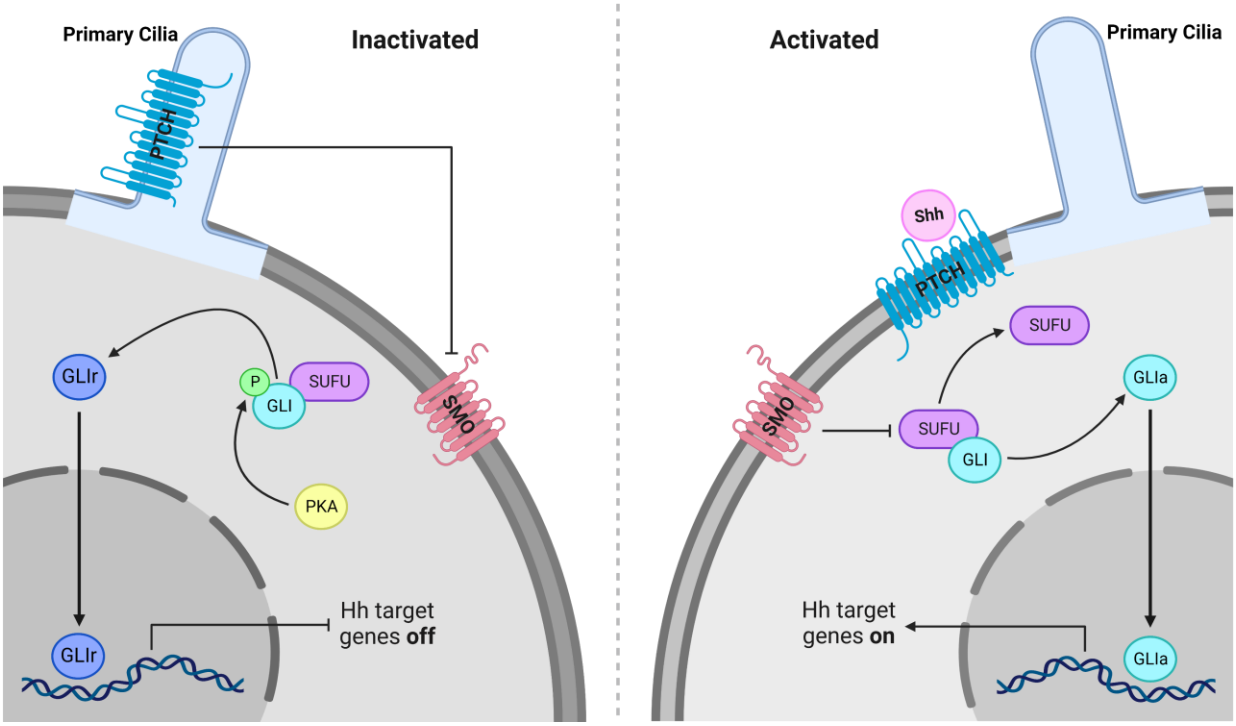

The Sonic Hedgehog (SHH) signaling pathway plays a critical role in SHH-activated MB tumorigenesis. The SHH signaling pathway plays an essential role in the control of GNPC proliferation in the EGL and is believed to drive tumor initiation in SHH MB. When SHH is not present, the Patched (PTCH) receptor is located inside primary cilia and plays an inhibitory role repressing SHH signaling. In the absence of SHH, GLI2 and GLI3 are phosphorylated leading to proteolytic cleavage to generate their repressor forms. When PTCH is located outside of primary cilia SHH binds to PTCH which releases the inhibitory effect PTCH has on Smoothened (SMO). De-inhibition of SMO results in activation of GLI transcription factors. Suppressor of fused (SUFU) is found in the cytoplasm and nucleus and plays a role in sequestering GLI proteins when SHH is not bound to PTCH. Binding of SHH to PTCH leads to inhibition of SUFU resulting in translocation of activated GLI to the nucleus.

Adapted from *"Hedgehog Signaling Pathway",* BioRender.com (2021).

Demographics and Prognosis

SHH MB tumors make up approximately 28% of all MB diagnoses and have an intermediate prognosis[13]. The 5-year overall survival (OS) rate in infants is 77%, in children is 68% and in adults is 75%[78]. This survival difference between age groups is likely attributed to the high percentage of infant SHH tumors that exhibit desmoplastic and extensive nodularity, which has been shown to be a positive prognostic factor in these young patients[79]. The majority of all SHH tumors are described as either having classic or desmoplastic/nodular histology with the remainder being large cell/anaplastic histology[4,13]. SHH MB displays a bimodal age distribution with the majority of cases occurring in both infants, which are patients younger than 3 years of age and adults, which are patients older than 17 years of age with fewer cases being diagnosed during childhood and adolescence[13,23]. A previous study showed that mutations in Tumor protein 53 (*TP53*) are found in 21% of all SHH MB tumors and that 72% of these patients aged 5 or older harboring this mutation succumbed to their disease[62]. This study identified *TP53* mutation as the most important independent risk factor in SHH MB. Li-Fraumeni syndrome is an inherited familial condition that is caused by a mutation in the tumor suppressor gene *TP53*[80]. Individuals with this syndrome are predisposed to a wide range of cancers including SHH MB.

SHH MB Cell of Origin

SHH signaling plays an important role in the proliferation of granule neuron progenitor cells (GNPCs) in the external granular layer during normal development of the cerebellum. During the development of the cerebellum, neurons are derived from a population of progenitor cells located in the external granule layer of the cerebellum named GNPCs[4]. Aberrant SHH signaling

may result in prolonged proliferation of GNPCs in the external granular layer, which is the region of the brain where SHH tumors are located. Schüller et al.[81] demonstrated that both early multipotent progenitors such as GFAP+ and Olig2+ cells and late unipotent progenitors such as Atoh1+ and Math1+ cells of the cerebellum can give rise to SHH MB. Similarly, Yang *et al*.[82] showed that deletion of *Ptch* and over activation of the SHH pathway can result in SHH MB in both neural stem cells and GNPCs. However, this can only occur after commitment to, and expansion of the neuronal lineage. These studies show that SHH MB can develop from neural stem cells or GNPCs of the cerebellum. These data provide evidence that GNPCs are the cell of origin for SHH MB[81,82]. Recently, Zhang et al. have shown that OLIG2+ progenitor cells can drive SHH MB tumorigenesis in mice, and these cells are enriched in recurrent or resistant SHH MB[83]. Researchers used single-cell transcriptomic analyses to demonstrate a developmental hierarchy of progenitor cells in SHH MB and identified OLIG2+ glial progenitors as transit amplifying cells at tumorigenic onset[83]. OLIG2+ progenitor cells are quiescent stem-like cells in fully developed MB but become active during relapse and are highly enriched in therapy resistant and recurrent SHH MB. These results demonstrate that OLIG2+ glial progenitor cells are critical tumor initiating cells during MB tumorigenesis and relapse that could have important implications for the design of therapies to target cell lineage vulnerability during MB tumorigenesis and recurrence[83].

SHH MB Subtypes

Recent studies have provided further insight into the heterogeneity within the SHH subgroup at the genetic and molecular level which has led to the discovery of additional subtypes within SHH MB[62]. Cavalli et al.[24] have determined that the SHH subgroup can be further subdivided into 4 distinct subtypes: SHHα, SHHβ, SHHγ and SHHδ. Most recently, the WHO

classification of Central Nervous System Tumors has redesignated the SHH MB subtypes according to the age of diagnosis as SHH-1 (-β), SHH-2 (-γ), SHH-3 (-α), and SHH-4 (-δ) (**Table 5**)[5]. Specifically, SHH-1 and SHH-2 correspond to infant subtypes while SHH-3 and SHH-4 correspond to childhood and adult subtypes, respectively[2]. The two infant subtypes are broken up based on prognosis. The SHH-1 subtype has a lower 5-year survival rate compared to the SHH-2 subtype which has a better prognosis[24].

Additionally, these subtypes can be further distinguished based on their genomic alterations and mutations. For example, SHH-3 tumors are enriched for *GLI2* and *MYCN* amplifications as well as *TP53* mutations, which have been shown to confer a poor prognosis compared to SHH-4 tumors which express *PTCH1* mutations and display a more favorable outcome[62]. Adult SHH MBs, which are mostly categorized as SHH-4, are characterized by a higher prevalence of SHH pathway associated mutations, including *PTCH1* and *SMO* alterations[66]. Additionally, several studies have demonstrated that telomerase reverse transcriptase (*TERT*) promoter mutations are found in SHH MB and are mainly associated with adult patients of the SHH-4 subtype[84-86].

Table 5: The Sonic Hedgehog (SHH) medulloblastoma subtypes

Subgroup		**SHH**			
Subtype		**SHH-1**	**SHH-2**	**SHH-3**	**SHH-4**
Demographics	Frequency (%)	16	21	29	34
	Age (years old)	0-3	0-3	>3-10, >10-17	17+
	% male : % female	47% : 53%	55% : 45%	63% : 37%	69% : 31%
Clinical features	Histology	Desmoplastic > classic	Desmoplastic > MBEN classic	Classic > Desmoplastic > LCA	Classic > desmoplastic
	Metastases	33%	8.9%	20%	9.4%
	Survival	67%	88%	70%	89%
Molecular features	Driver events	*PTCH1* mutation *SUFU* mutation/ deletion *PTEN* deletion	*PTCH1* or *SMO* mutation *PTEN* deletion	*MYCN* or *GLI2* amplification *TP53* mutation *PTCH1* mutation	*PTCH1* mutation *TERT* promoter mutation

The Sonic Hedgehog (SHH) MB subgroup is divided into 4 different subtypes based on demographics, clinical features and molecular features: SHHα, SHHβ, SHHγ and SHHδ. Most recently, the WHO classification of Central Nervous System Tumors has redesignated the SHH MB subtypes according to the age of diagnosis as SHH-1 (-β), SHH-2 (-γ), SHH-3 (-α), and SHH-4 (-δ).

Adapted from Hovestadt et al. *Nature Reviews Cancer,* 2019 and Cavalli et al., *Cancer Cell,* 2017.* New designations based on WHO Classification of Central Nervous System Tumors, 2021.

SHH MB Cell Models

Unfortunately, very few SHH MB cell lines exist, making this tumor difficult to study *in vitro*. SHH MB tumors are very hard to culture, and very few models are available for *in vitro* assessments. The Daoy cell line is over 35 years old[87], has been shown to exhibit global activation of SHH-pathway genes and is statistically classified as the SHH subtype[88]. UI226 cells are a low passage patient-derived cell line[89] and have been designated SHH MB through transcriptome profiling[90]. Low passage patient derived cell lines are more clinically relevant and provide an excellent complementary model to cultured cell lines such as Daoy. Patient derived cell lines better recapitulate and sustain the molecular alterations expressed in human tumors, which explains why they are more clinically relevant and preferred. In addition, culturing cells in suspension as tumorspheres has been shown to provide a highly biologically relevant *in vitro* model system for investigating drug responses (**Fig. 4**). These 3D brain tumor cultures are grown in defined serum free conditions and better recapitulate the phenotypic and genotypic changes observed in primary tumors than cells grown in serum as adherent cultures[91]. In this assay, individual cells are cultured in ultra-low attachment plates. They are then incubated undisturbed, and after 5-7 days tumorspheres are counted and measured. These are called primary tumorspheres as they have only been passed one time. These primary tumorspheres can be dissociated, plated, recounted, and re-measured after another 5-7 days. These are secondary tumorspheres as they have been passed for a second time. Theoretically, only a stem cell will give rise to a new sphere so changes in tumorsphere number reflect changes in stem cell self-renewal capacity[91]. This is an important factor to consider because theoretically, if self-renewal capacity can be attenuated, then new tumors cannot form if they are driven by cancer stem cells. Additionally, changes in tumorsphere size reflect changes in cell proliferation, cell size or cell adhesion capacities[91].

Figure 4. The tumorsphere assay

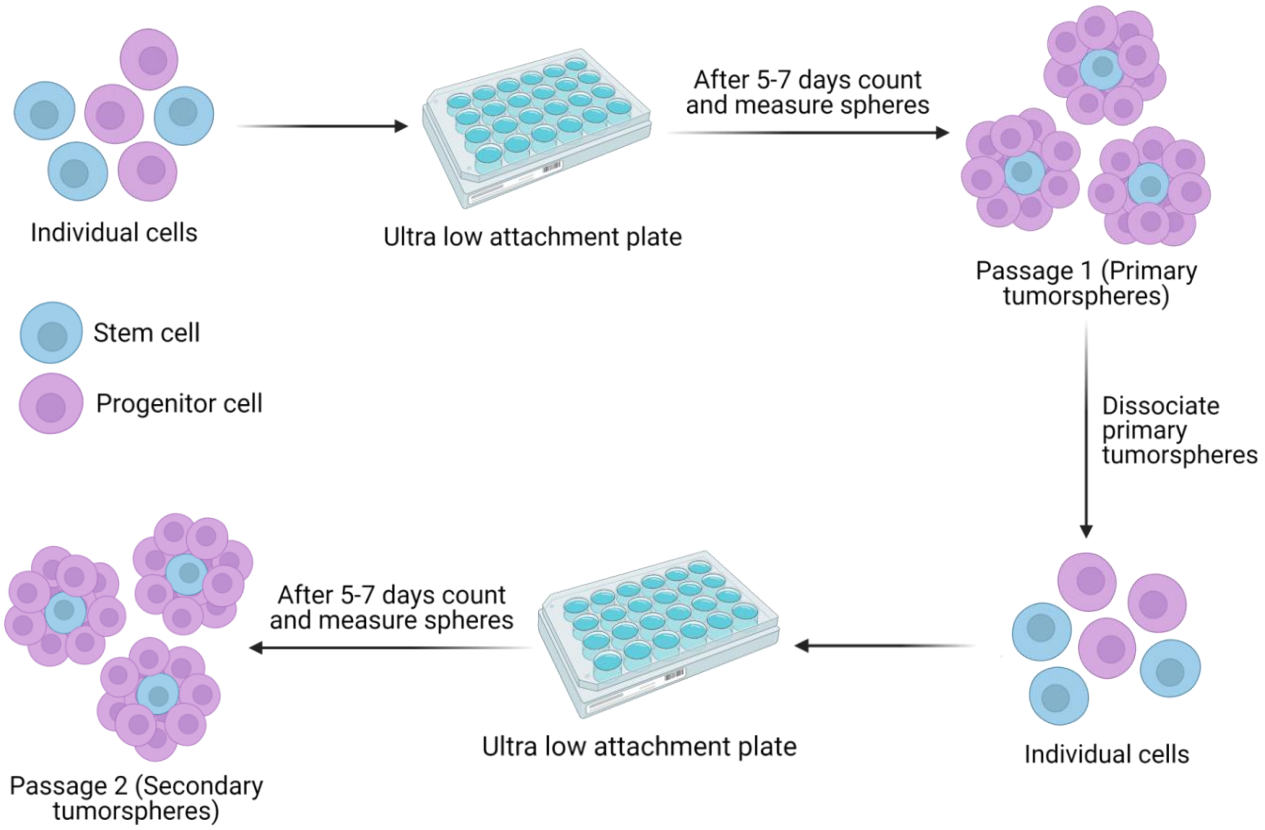

UI226 (5000 cells/well) and Daoy (10 000 cells/well) cells are plated into each well of a 24-well ultra-low attachment plate in the presence of various concentrations of selumetinib or trametinib. They are then incubated undisturbed at 37°C for 7 days (UI226) or 5 days (Daoy) and are then counted and measured. These are called primary tumorspheres as they have only been passed one time. These primary tumorspheres can be dissociated, plated with varying concentrations of drug again and recounted and re-measured after another 5-7 days. These are secondary tumorspheres.

SHH MB Mouse Models

Several genetically engineered mouse models have been generated to study SHH MB tumor initiation and progression *in vivo*. SHH mouse models are typically generated by genetic manipulations of SHH pathway genes since mutations in the SHH signaling pathway represent the most common genetic events observed in these tumors. Deletion of *PTCH1* or *SUFU*, as well as activation of *SMO* in mice results in tumors that resemble human SHH MB[92-94]. Mouse xenograft models are also used where cultured human SHH MB cells are injected into the cerebellum of immunodeficient mice. Human SHH MB cells are typically grown in nonobese diabetic severe combined immune deficiency (NOD SCID) or nonobese diabetic severe combined immune deficiency gamma (NSG) mice. NOD SCID mice have defective macrophages and dendritic cells and lack both T cells and B cells, whereas NOD SCID Gamma (NSG) mice also lack natural killer cells. NSG mice are one of the most immunodeficient mouse strains allowing human tumor cells to successfully engraft and grow. Patient derived xenograft (PDX) lines are generated by implanting patient cells directly into the cerebellum of immunodeficient NSG mice and propagating them from mouse to mouse without *in vitro* passaging. PDX models are considered to be "gold standard" *in vivo* models as they have been shown to maintain the characteristics of the primary human tumor from which they were derived. For example, RCMB18 cells are patient derived SHH MB cells. These cells exhibit loss of *TP53*, *MYCN* amplification and a SMO mutation designating these cells as the SHH subgroup[66,95]. However, recent studies have shown variability in blood-brain-tumor barrier (BBTB) integrity between PDX models and genetically engineered mouse models[96]. A critical consideration and major hurdle during the development and administration of novel brain tumor therapies is the impaired delivery of drugs to the tumor cells due to the specialized endothelial blood-brain barrier (BBB). The BBB varies across the different

MB subgroups. For example, the WNT subgroup has a very leaky BBB, which allows ample drug and chemotherapeutics to reach the tumor. In contrast, SHH and Group 3 patients have a heterogeneous BBB and Group 4 patients exhibit a completely intact BBB making this an important variable to consider when evaluating drugs for the treatment of these different subgroups. Drug delivery across the BBTB is critical for successful translation of novel therapies to treat MB. Genovesi et al.[96] showed that SHH MB genetically engineered mouse model tumors present with a completely intact BBTB compared to PDX models of SHH MB tumors, which display a heterogeneous BBTB. This heterogeneity could be due to the surgery or tumor cell injection, which could damage or disrupt the BBTB. This also could be attributed to the genetics of these mice and their significant immunodeficiency that could cause the BBTB to be altered in these models. However, these PDX models are representative of the BBTB observed in patients with SHH MB and are therefore representative of the human tumors from which they were derived. These findings question the translational relevance of some SHH MB mouse models and highlight the importance of characterizing the functional status of the BBTB in preclinical models of MB. These data also suggest that depending on the MB subgroup, PDX mouse models may not necessarily be the "gold standard" mouse models to evaluate the effect of therapies to treat MB and support the idea that multiple models should be utilized for brain tumor studies.

Treatment of SHH MB in the molecular age

Activation of the SHH signaling pathway in SHH MB has been extensively studied and is the basis for the design and development of targeted therapies to treat this subgroup. Accordingly, SMO inhibitors such as cyclopamine and vismodegib have been evaluated in MB patients with SHH pathway activation[97]. These small molecule inhibitors suppress SHH signaling by binding to

SMO[98,99]. Vismodegib and other SMO inhibitors have previously been tested in Phase I and Phase II clinical trials for the treatment of MB[100-102]. The results of these studies determined that vismodegib produced a low overall response rate that ultimately did not result in a significant survival increase in SHH MB patients. Additionally, some other SMO inhibitors such as sonidegib have initially been successful in reducing tumor burden in some SHH MB tumors, but ultimately the patients eventually relapse due to drug resistance. This is partially attributed to mutations that arise in downstream targets such as *SUFU* and activation of *GLI* in the absence of SMO[66,97,103] accounting for the variable responses between the SHH MB subtypes. Kool et al.[66] and Remke et al.[104] have demonstrated that SHH pathway antagonists work on adult tumors from the SHH-4 subtype that have mutations in upstream pathway targets such as *PTCH1* or *SMO*. However, these antagonists do not work on infant or child tumors from the other subtypes with mutations in downstream signaling targets such as *SUFU* or *GLI.* GLI mutations are particularly resistant to SHH pathway inhibitors and patients with *TP53* mutations are resistant to vismodegib treatment[62]. Therefore, SHH-3 tumors have the worst prognosis and are completely resistant to SHH pathway antagonists as they are enriched for *MYCN* amplification, *GLI2* amplification and *TP53* mutations. Morrissy et al. have shown that genetic events in a mouse model of recurrent SHH MB exhibit poor overlap with the matched primary tumors[105]. Whole genome-sequencing in human samples also demonstrated that the genetic mutations present in the tumor at the time of diagnosis were different than the genetic events present following treatment[105]. Therefore, targeted therapies against the primary tumor will most likely be ineffective against recurrent tumors that have loss of function of TP53. Thus, targeted therapies that have the potential to reduce toxicity and improve survival are urgently needed.

MAPK signaling in SHH MB

SHH MB tumors also exhibit upregulation of other signaling pathways. Therefore, crosstalk between pathways also plays a role in treatment resistance. In fact, the Ogilvie lab has recently identified novel roles for the CD271/p75 neurotrophin receptor and the MEK/ERK signaling pathway (**Fig. 5**) in contributing to SHH MB growth and tumor progression[106]. Bioinformatics analyses of large patient datasets and tumorspheres from SHH MB cultures were performed and demonstrated that SHH MB cells exhibit elevated MAPK activity[106,107]. The MAP kinase pathway promotes cell proliferation and cell survival. Aberrant activation of the Raf/MEK/ERK protein kinase cascade is often detected in human cancers[108]. Dysregulated activity of the MAPK signaling pathway drives uncontrolled tumor cell proliferation and tumor growth. The MAPK pathway is therefore an important therapeutic target for the treatment of many different cancers including SHH MB. Particularly, MEK inhibitors (MEKi's) have been the most successful small molecular weight inhibitors for targeting the MAPK pathway[108]. MEK1/2 have unique characteristics that make them excellent targets for therapeutic development. For example, MEK1/2 have very narrow substrate specificity which means that MEKi's can specifically inhibit ERK1/2 signaling without directly affecting any other signaling pathways[108]. MEK1/2 proteins also have a unique structure which allows for the design of highly selective ATP-noncompetitive inhibitors. ATP-noncompetitive inhibitors, also known as allosteric inhibitors, bind at a site different than the ATP-binding pocket and induce a conformational change that locks MEK1/2 into an inactive state[108]. This results in very specific inhibition and a relatively low chance that the inhibitor will induce undesired effects. Several highly selective and potent MEKi's are available and currently being tested for their therapeutic potential.

Figure 5. The MAPK signaling pathway and selumetinib and trametinib inhibition

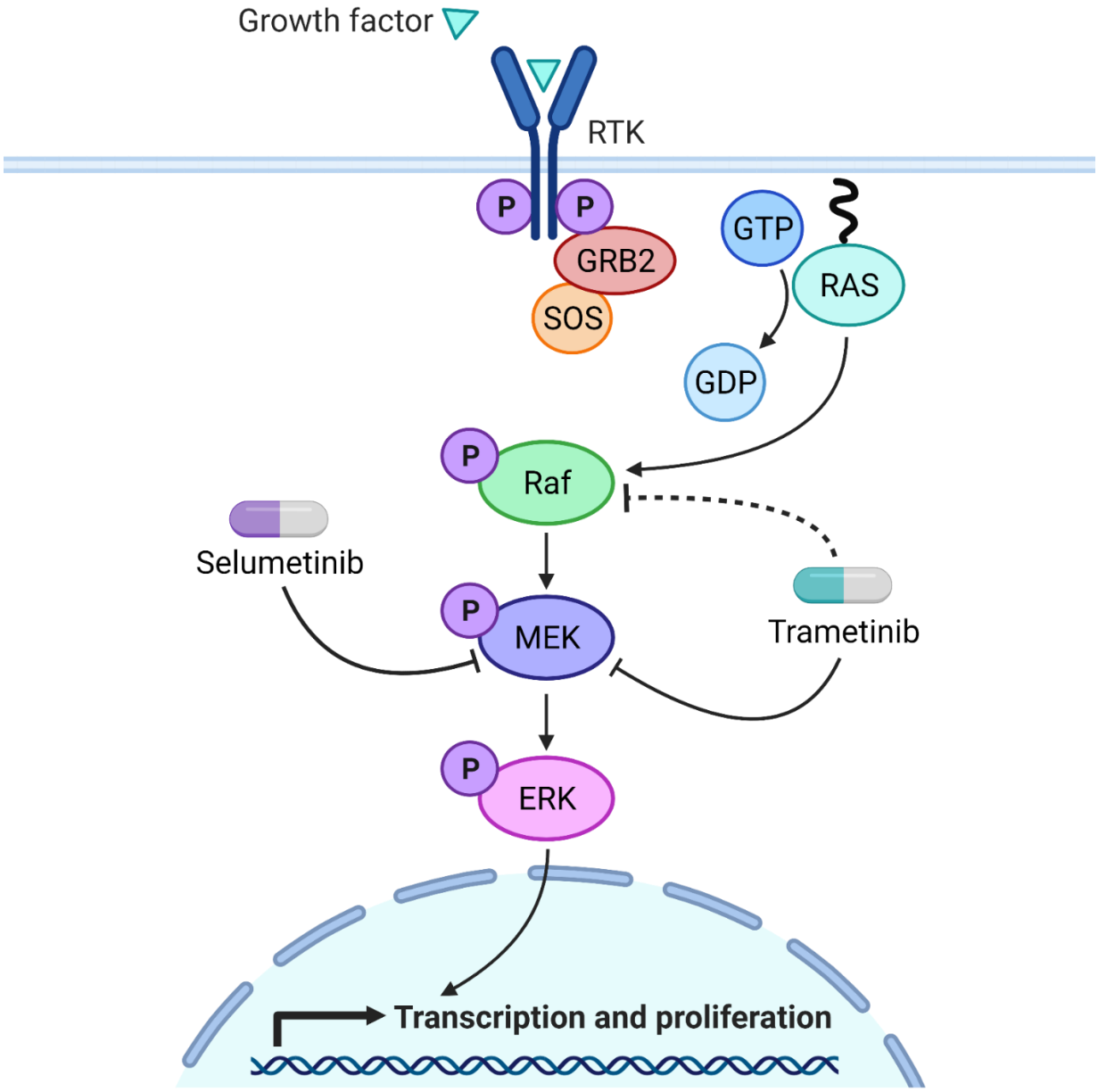

The mitogen-activated protein kinase (MAPK) pathway is also known as the Ras-Raf-MEK-ERK pathway which promotes cell proliferation and survival. A growth factor binds to receptor-linked tyrosine kinase (RTK) activating the cytoplasmic domain. RTK becomes phosphorylated allowing the GRB2-SOS complex to bind and become activated. Ras is activated by GTP which then activates Raf triggering the protein kinase cascade. Selumetinib is an allosteric inhibitor that inhibits enzymatic activity of MEK1/2 but not MEK1/2 phosphorylation by Raf. Trametinib is also a highly selective allosteric inhibitor that induces allosteric inhibition of MEK1/2 catalysis. Trametinib also causes MEK1/2 to dissociate from Raf which further inhibits ERK1/2 phosphorylation.

Adapted from *"Raf Pathway"*, BioRender.com (2021).

The MEKi Selumetinib

The MEKi selumetinib is blood brain barrier penetrant and has undergone extensive clinical testing for the treatment of other pediatric cancers such as plexiform neurofibromas[109,110] and refractory low-grade gliomas[111,112]. Importantly, it has shown excellent tolerability in both diseases. Selumetinib is an allosteric inhibitor that directly inhibits the enzymatic activity of MEK1/2 but does not affect the phosphorylation of MEK1/2 by Raf (**Fig. 5**)[108]. Molecular modeling has suggested that selumetinib binds to a unique allosteric site in MEK1/2, which confers a high selectivity. Previous studies have demonstrated that selumetinib robustly inhibits ERK1/2 phosphorylation in *RAS* or *BRAF* mutant tumors, and has been shown to elicit its antitumor activity in a number of different cancer xenograft models including liver, skin, lung, colorectal, and pancreatic[108]. Additionally, a phase II clinical trial has demonstrated that selumetinib exhibits significant efficacy when used to treat tumors that have high MEK/ERK activity such as recurrent low-grade serous carcinoma of the ovary or peritoneum as well as biliary cancers[108]. Our lab has also evaluated the effect of selumetinib on SHH MB tumorigenic properties both *in vitro* and *in vivo*[106]. Selumetinib treatment did not have an effect on tumorsphere formation, but it did decrease tumorsphere size and cell viability *in vitro*[106]. Importantly, selumetinib treatment significantly extended survival in a preclinical xenograft model[106]. These results provided the first evidence that the MEK/ERK signaling pathway is a therapeutic target in human SHH MB. The MAPK signaling pathway has also recently been shown to drive SHH pathway inhibitor resistance. Zhao et al.[113] determined that the MAPK signaling pathway is increased in metastatic SHH medulloblastoma. While Liang et al.[106] showed that selumetinib treatment significantly extends survival in an intracerebellar transplant model of SHH MB, the mice ultimately succumb to disease progression. Our lab has since evaluated the effect of selumetinib in combination with other signaling pathway

inhibitors. Zagozewski et al.[114] performed RNA sequencing on selumetinib treated xenografts to identify molecular pathways that were differentially expressed following MEK inhibition. We determined that the JAK/STAT3 signaling pathway was upregulated following selumetinib treatment and that treatment with selumetinib in combination with the JAK/STAT3 pathway inhibitor pacritinib further reduced tumor growth and significantly increased survival *in vivo* compared to either inhibitor alone. This appears to be a promising new strategy to fight SHH medulloblastoma, however, there are other MEKi's that are considered "best in class" or more potent than selumetinib. These should also be evaluated either alone or in combination with other signaling pathway inhibitors as potential new therapeutic options to treat SHH MB.

Trametinib is a more potent MEKi

The more potent MEKi trametinib is approved for adult BRAF V600E mutant cancers and is also currently undergoing evaluation in both refractory low-grade gliomas and plexiform neurofibromas (NCT03363217, NCT02124772)[115,116]. Trametinib is also a highly selective allosteric inhibitor that does not compete with ATP or ERK1/2 to induce allosteric inhibition of MEK1/2 catalysis. Interestingly, trametinib causes MEK1/2 to dissociate from C-Raf which further inhibits ERK1/2 phosphorylation[108]. Therefore, trametinib not only inhibits MEK1/2 activity but also Raf activation of MEK1/2 which increases the potency of this inhibitor (**Fig. 5**)[108]. Importantly, Manoharan et al.[117] and Selt et al.[118] recently completed clinical trials to evaluate trametinib for the treatment of recurrent/progressive pediatric low-grade gliomas[117,118]. These studies reported favorable results and the findings support the use of trametinib as an effective treatment for recurrent/progressive pediatric low-grade gliomas. However, both clinical trials reported minor side effects from trametinib treatment including skin toxicity which ranged in

severity from a mild rash to a more significant inflammatory eruption. This skin toxicity caused small, raised, acne-like bumps to form on the face, scalp, chest, and upper back. These side effects were treated either with topical or systemic antibiotics[117,118]. These findings are consistent with side effects reported from other MEKi studies which ultimately have not prevented the use of MEKi's as potential therapy options. Additionally, trametinib has showed efficacy in patients with non-small cell lung carcinoma, pancreatic cancer, and *NRAS* mutant melanoma. While selumetinib and trametinib have excellent toxicity profiles in children, to our knowledge, trametinib has not been tested in preclinical models of MB and particularly on the SHH subgroup. Thus, the first aim of my thesis is to evaluate the effect of the "best in class" MEKi, trametinib on tumorigenic properties *in vitro* and the second aim is to perform pilot studies to evaluate its effect on tumor growth *in vivo.* I hypothesize that trametinib will significantly decrease SHH MB tumorigenic properties including stem cell proliferation, survival, and migration *in vitro* while also decreasing tumor growth *in vivo*.

Chapter II: Materials and Methods

Cell culture and *in vitro* drug treatments

All *in vitro* experiments were performed using UI226 low passage primary SHH MB cells as well as the established cell line Daoy[87]. UI226 cells were a gift from Dr. Timothy Ryken (Dartmouth-Hitchcock Medical Center, New Hampshire, USA) and were propagated in StemPro media as previously described[106,119]. NanoString analysis was used to classify UI226 cells as SHH MB[90]. Daoy cells were purchased from ATCC and cultured as previously described[89,106]. Short Tandem Repeat profiling (ATCC) was used to authenticate all cell lines used in this study. The tumorsphere assay was used to evaluate the effect of selumetinib and trametinib on both cell lines. Briefly, UI226 (5,000 cells/well) and Daoy (10,000 cells/well) cells were plated into each well of a 24-well ultra-low attachment plate (Corning, New York, USA) and grown in StemPro media[106,119] (UI226) or neural precursor media (Daoy) which consists of DMEM F12, B27 (50x), N2 (100x), 10 µg/mL bFGF and 10 µg/mL EGF. Selumetinib (MedChemExpress, Monmouth Junction, New Jersey, USA) was added at 1 µM, 5 µM, 10 µM, 20 µM and 50 µM to the cells. Trametinib (MedChemExpress) was added at 50 nM, 100 nM, 250 nM, 500 nM or 1 µM to the cells. DMSO served as the vehicle control. Tumorspheres were incubated undisturbed at 37°C, 5% CO_2 for 7 days (UI226) or 5 days (Daoy), counted and measured. Tumorsphere number, tumorsphere size, cell viability and total cell number were evaluated and compared to DMSO controls. Fiji/ImageJ was used to evaluate individual tumorsphere size in multiple wells per treatment group. Results were displayed as cumulative frequency distribution of tumorsphere area. Only tumorspheres greater than 25 µm were included in these analyses[114]. Cell viability was assessed using a TC20 cell counter (BioRad, California, USA) by dissociating primary tumorspheres and mixing 10 µL of cells with 10 µL of Trypan Blue.

For immunoblotting analysis, $2x10^5$ cells/well were plated into each well of a six-well ultra-low attachment plate in the presence of drug as described above. Cells were collected after 3 days, and protein was extracted for immunoblotting.

Immunoblotting

UI226 and Daoy tumorspheres were grown in culture and treated with selumetinib or trametinib as described above. Protein was isolated from dissociated primary tumorspheres using 975 μL of Lysis Buffer (25 mM Tris pH 7.4, 150 mM NaCl, 1% Triton X-100, 5 mM EDTA, 1x protease inhibitor, and 1 mM sodium pervanadate), 20 μL of 50x protease inhibitor (Sigma-Aldrich, St. Louis, Missouri, USA), and 5 μL of 200 μM sodium orthovanadate. Protein quantities ranging from 20-30 μg were loaded onto 12% Tris-glycine gels and resolved by SDS–PAGE. Protein was transferred using a semi-dry transfer method to nitrocellulose membranes (Bio-Rad) and washed as previously described[89,106]. Membranes were blocked with 5% milk in 1x TBST for one hour at room temperature and then incubated overnight at 4°C in primary antibodies (**Table 6**). The following day, membranes were washed 3x with 1x TBST for 5 min and then secondary antibodies (**Table 6**) conjugated to horseradish peroxidase were added for one hour at room temperature. Signal detection was performed using SuperSignal West Pico (ThermoFisher Scientific, Waltham, Massachusetts, USA) and blots were imaged using a Fusion FX Vilber Lourmat chemiluminescent imaging system (Marne LA Vallee Cedex 3, France).

Table 6: List of antibodies used for immunoblot analysis

Name	Company/Catalogue number	Dilution
Primary antibodies		
P-ERK	CST (4370)	1/1000
ERK	CST (4695)	1/1000
GAPDH	Santa Cruz (sc47724)	1/1000
Secondary antibodies		
Goat anti-mouse HRP	Abcam (ab6789)	1/3000
Donkey anti-rabbit HRP	Jackson ImmunoResearch (711-035-152)	1/5000

Migration assay

Daoy and UI226 cells were plated in 96-well ultra-low attachment round-bottom plates at 10,000 cells/well and 4,000 cells/well, respectively and left to aggregate or form spheroids over 4 days. They were then overlain with a Type I collagen mixture (Collagen type I (Corning, New York, USA), DMEM, and NaOH). 100 µL of medium was removed and replaced with 100 µL of the collagen mixture. Once the collagen had solidified, 100 µL of medium containing DMSO or 50 nM, 100 nM, 250 nM, 500 nM or 1 µM of trametinib was added. Migration was assessed after 3 days by subtracting the day 0 diameter from the diameter of the migration front measured at day 3.

Intracerebellar transplantation and drug treatment

All procedures were approved by the University of Manitoba Animal Care Committee. NOD SCID mice were administered 0.1 mL of either 0.5 mg/kg, 1.0 mg/kg or 1.5 mg/kg of trametinib to evaluate drug toxicity over 28 days. Each treatment group consisted of 2 mice that were given drug once daily via oral gavage on a 5 day on, 2 day off schedule. UI226 SHH MB cells were cultured as tumorspheres, dissociated and $2.5x10^5$ cells/animal were intracerebrally injected into the cerebellum of 7-9 week old immunodeficient NOD SCID mice[54,58,89,106,120,121]. Group 3 MB HDMB03 cells were obtained from Dr. Till Milde[122], cultured as previously described[57] and $5x10^4$ cells/animal were intracerebrally injected into the cerebellum of 7-9 week old immunodeficient NOD SCID mice. RCMB18 cells exhibit loss of *TP53*, *MYCN* amplification and a *SMO* mutation[95,123] designating these cells as the SHH subgroup. Patient derived SHH MB RCMB18 cells were thawed and $3x10^5$ cells/animal were intracerebrally injected into the cerebellum of immunodeficient NOD SCID IL2Rg null (NSG) mice. Following tumor

engraftment, the animals were randomly split into two groups with one receiving either 0.5% hydroxypropyl methyl cellulose, 0.1% polysorbate 80 as the vehicle control or 1.5 mg/kg of trametinib. Treatment was administered via oral gavage on a 5 day on, 2 day off schedule following tumor engraftment. Animals were treated until they reached endpoint (mice could no longer walk or groom themselves properly or had lost 20% of their peak weight). Animals were then perfused, and their brains were extracted and used either for RNA sequencing or histological analysis. The mice were held according to the Guidelines of the Canadian Council on Animal Care and the Animal Care and Use Policy of the University of Manitoba. Briefly, they were kept housed in IVC caging (Tecniplast) with bedding that had been sterilized by steam autoclave. The light cycle of the room began with lights on at 6:00 a.m. and continued on a 12 hr on and 12 hr off schedule. The room temperature was kept between 21–23°C and had a humidity target of 50%. MRI was performed on a MR Solutions cryogen free FlexiScan 7 T system (MR Solutions, Guildford, Surrey, UK) as previously described[57,106]. During the procedure, mice were anaesthetized with 4% isoflurane and maintained with a mask at 1.5%–2% isoflurane in oxygen.

RNA-sequencing

To identify aberrant molecular changes following trametinib treatment, we performed RNA sequencing on drug treated UI226 SHH MB tumorspheres as well as on UI226 xenograft mice tumors. UI226 tumorspheres were plated at $2x10^5$ cells/well into each well of a six-well ultra-low attachment plate. DMSO control or 250 nM of trametinib was added to the tumorspheres and samples were collected after 3 days (N=4) or 7 days (N=4) for RNA extraction. For the *in vivo* study, once UI226 xenograft mice reached endpoint, tumors were resected, and human cells were isolated using a brain tumor dissociation kit (Miltenyi Biotec, Bergisch Gladbach, North Rhine-

Westphalia, Germany) followed by a mouse cell depletion kit (Miltenyi Biotec) according to manufacturer's instructions. RNA was extracted from 3 vehicle control endpoint tumors taken at days 61, 63 and 65 and from 3 trametinib-treated xenografts at endpoint taken at days 75, 76 and 80. RNA was extracted using the Norgen RNA extraction kit (Norgen Biotek, Thorold, ON, Canada) according to manufacturer's instructions. Library preparation and RNA sequencing were performed by StemCore laboratories at the Ottawa Hospital Research Institute (Ottawa, ON, Canada) as previously described[57,106]. Libraries were prepared from 500 ng of input total RNA with the Truseq RNA v2 library prep kit (Illumina). RNA sequencing was performed comparing control and trametinib treated tumor cells from primary xenografts.

Xenograft libraries

Reads from xenograft tumor RNA-seq libraries were mapped to the human reference genome (GRCh38 assembly) guided by transcripts from GENCODE release 35, and separately to the mouse reference genome (GRCm38 assembly) guided by transcripts from GENCODE release M25, using hisat2 2.2.1. Human and mouse BAM files were passed to XenofilteR (v1.6) to identify and remove reads that map more closely to the mouse genome, and that are thus considered to originate from the mouse host. The remaining (presumed human graft origin) reads were quantified with salmon v.1.4.0[124]. Salmon provides fast and bias-aware quantification of transcript expression[124] against an index built from the GENCODE v35 assembly with inclusion of genomic decoy sequences. Data were loaded into R using the tximport library and the gene/count matrix was filtered to retain only genes with five or more mapped reads in two or more samples. Differential expression was assessed using DESeq2 (v1.30.1), comparing the two conditions (vehicle control and trametinib-treated). Principal component analysis (PCA) was performed using

the DESeq2 plotPCA function, and hierarchical clustering was run using Euclidian distance; both using rlog-transformed count data. Expression differences between control and trametinib-treated samples were calculated using the DESeq results function with an alpha value of 0.05, and estimated fold changes were shrunk with the lfcShrink function using the apeglm method. Lists of significantly differentially expressed (DE) genes were identified using a q-value (Benjamini-Hochberg corrected p-value) cut-off of 0.05, (corresponding to a p-value of ~0.00025).

Tumorsphere libraries

Reads from control and trametinib treated tumorsphere RNA-seq libraries (3 days and 7 days 7 post treatment) were similarly quantified with salmon (v.1.7.0) against an index built from the GENCODE v35 assembly with genomic decoy sequences. Data from both timepoints and both controls (15 samples) were loaded into R and filtered as described for the xenograft samples. Expression differences were calculated between Trametinib-treated samples and their matched controls at each time point, again as described for the xenograft libraries.

Gene Set Enrichment Analysis

GSEA (v4.1.0) was run using pre-ranked gene lists (the GSEA_preranked method) to explore enrichment of pathways and functional classes in genes expression changes following trametinib treatment of xenografts and tumorspheres. The DE gene lists were filtered to retain protein-coding genes, and ranked by "-log10(p-value) * sign(fold change)". GSEA was run using the MSigDb (v7.4) collections H (hallmark gene sets), C2:CP (canonical pathways), C4:CGN (cancer gene networks), C4:CM (cancer modules), C6 (oncogenic signatures), and C8 (cell type signatures). Enrichment maps were generated in Cytoscape (v3.8.2) from GSEA results, following

the protocol described by Reimand et al.[125]. Enriched gene sets with a q value <0.005 were retained and clustered using the AutoAnnotate tool; figures were edited to remove unclustered gene sets, and small clusters unrelated to the cell types being studied.

Immunohistochemistry

Tumors from UI226, RCMB18 and HDMB03 xenografts were sectioned following formalin fixation and paraffin embedding. Slides were de-parafinized and re-hydrated in xylene and ethanol gradients followed by antigen retrieval in sodium citrate buffer at 95-100°C for 20 min. Slides were washed in 1x PBS and then treated for endogenous peroxidases for 10 minutes and again washed in 1x PBS. The samples were blocked in 3% sheep serum for 30 minutes at room temperature. They were then incubated with primary antibodies (**Table 7**) prepared in 1% sheep serum/1x PBS overnight at 4°C. The following day, the slides were first incubated in biotinylated secondary antibodies (**Table 7**) for 2 hours at room temperature. Streptavidin/HRP antibody (Jackson ImmunoResearch, West Grove, PA, USA) in 1x PBS was then added for 30 minutes at room temperature. Slides were then developed with DAB substrate (Sigma-Aldrich, St. Louis, Missouri, USA), counterstained with hematoxylin and mounted in Permount (ThermoFisher Scientific, Waltham, Massachusetts, USA).

Table 7: List of antibodies used for immunohistochemical analysis

Name	Company/Catalogue number	Dilution
Primary antibodies		
Anti-mitochondria	Abcam (ab92824)	1/500
p-ERK	CST (9101)	1/400
Secondary antibodies		
Biotin-SP goat anti-rabbit	Cedarlane (111-065-144)	1/500
Biotin-SP sheep anti-mouse	Jackson ImmunoResearch (515-065-003)	1/500

Statistical Analysis

Data from *in vitro* and *in vivo* experiments were analyzed using Prism 9.0 software (GraphPad Software). Xenograft survival data was evaluated using the log-rank (Mantel–Cox) test. Tumorsphere size analysis was performed using 2-sample Kolmogorov–Smirnov tests. One-way ANOVA followed by a Dunnett's test for multiple comparisons were used to assess total tumorsphere number, cell viability and cell migration. All data are reported as ± SEM. P values < 0.05 were considered significant.

Chapter III: Results

Trametinib significantly inhibits SHH MB tumor properties at nanomolar concentrations.

To assess the effect of trametinib on SHH MB cells, various drug concentrations were evaluated using the well-established tumorsphere assay (**Fig. 4**) and compared to an established range of previously tested selumetinib concentrations[106]. Tumorspheres are a highly biologically relevant *in vitro* model system for investigating drug responses[89,106,120]. These 3D brain tumor cultures are grown in stem cell-enriched conditions and better sustain the genotypic and phenotypic changes as well as the transcriptional programs observed in primary tumors than adherent cells grown in serum[57,126]. On-target effects for both selumetinib and trametinib were determined by immunoblot analyses following 3 days of drug treatment. Both selumetinib and trametinib elicited a dose-dependent decrease in p-ERK levels in UI226 tumorspheres (recently derived from a primary SHH MB tumor[89,119] and classified as SHH MB by NanoString analysis[90]) (**Fig. 6A-B**). Additionally, the MEKi's induced the same dose dependent response in Daoy[87] MB tumorspheres (**Fig. 6C-D**). This decrease was even observed at the lowest concentration of trametinib (50 nM) in tumorspheres from both cell lines.

Figure 6. Treatment with the MEK1/2 inhibitors decrease p-ERK1/2 levels

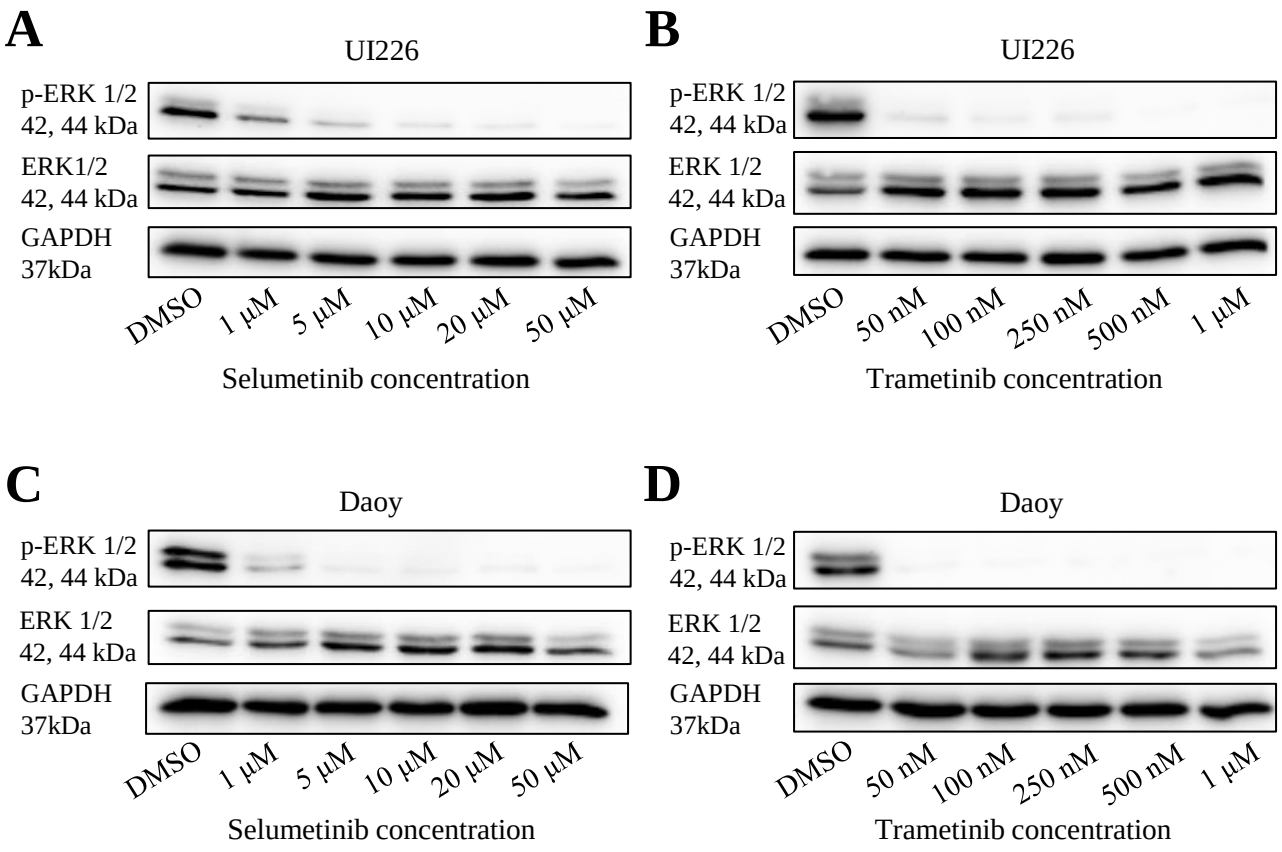

A-D) Western blot validation of decreased pERK1/2 levels in selumetinib treated primary UI226 tumorspheres (A), trametinib treated primary UI226 tumorspheres (B), selumetinib treated Daoy tumorspheres (C) and trametinib treated Daoy tumorspheres (D) after 3 days of treatment. Total ERK and GAPDH served as loading controls.

Next, the effects of selumetinib and trametinib on tumorsphere size were independently evaluated by cumulative frequency distribution analyses using Fiji/ImageJ**.** Both MEKi's significantly decreased UI226 and Daoy tumorsphere size (**Fig. 7A-D and 8A-D**) but had minimal effect on the overall number of UI226 or Daoy tumorspheres (**Fig. 9A-D**). However, a significant effect was observed on UI226 tumorsphere number at the highest concentration of selumetinib and on Daoy tumorsphere number at the highest concentration of trametinib. Both MEKi's significantly decreased UI226 and Daoy cell viability (**Fig. 10A-D**) with notable decreases starting at 10 μM for selumetinib and 250 nM for trametinib.

Having shown a strong inhibitory effect of trametinib on tumorspheres in the nanomolar range, we next assessed the effect of this more potent MEKi on cell migration in our 3D collagen assay. Both UI226 and Daoy exhibit a significant decrease in cell motility following treatment with trametinib (**Fig. 11A-B**). Collectively, these results demonstrate that trametinib is highly effective at inducing an overall decrease in SHH MB tumorigenic properties *in vitro*, including tumorsphere size, cell viability and migration.

Figure 7. Images depicting treatment with the MEK1/2 inhibitors decreases tumorsphere size

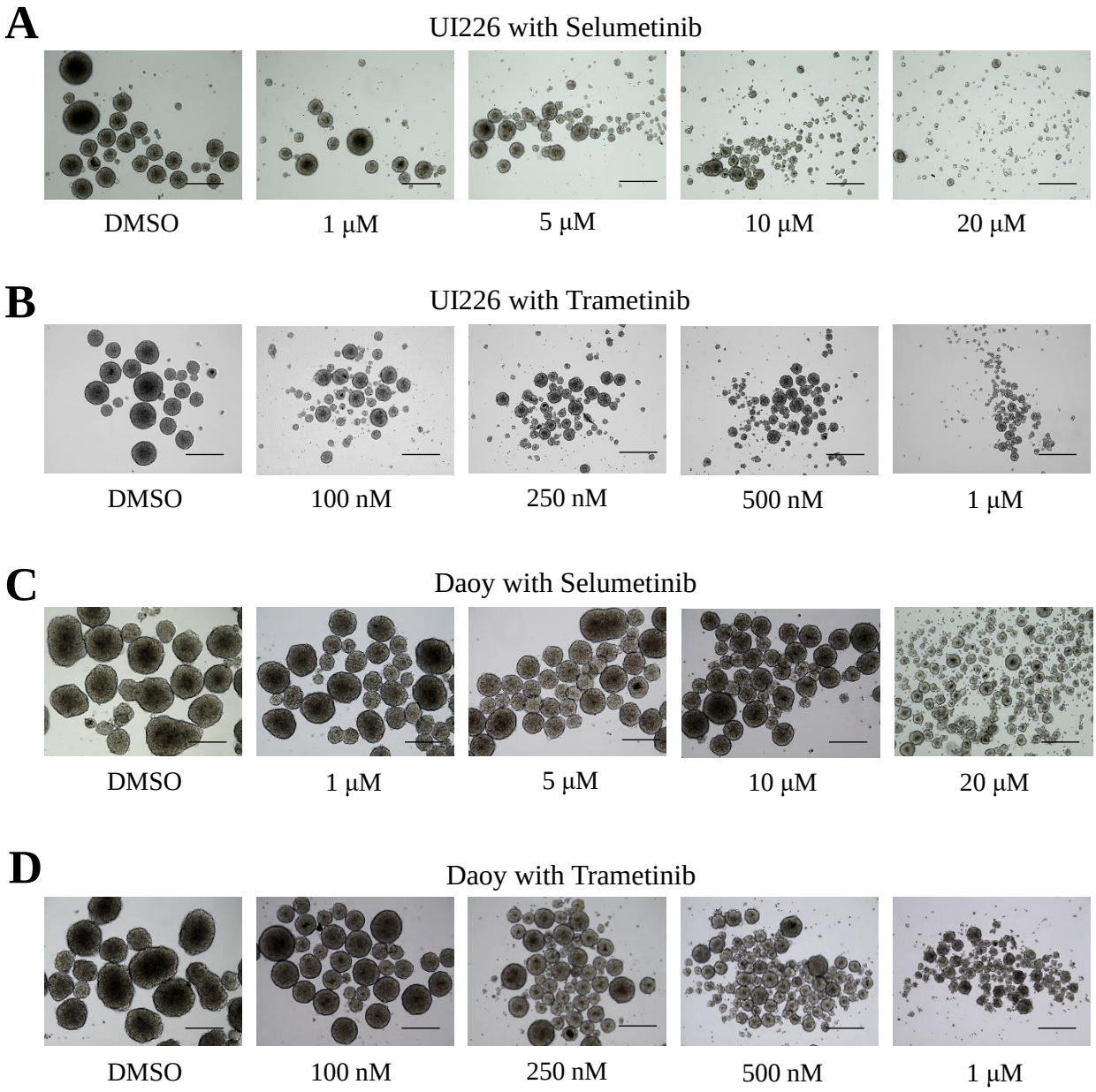

A-B. Representative images of UI226 tumorspheres following treatment with various concentrations of selumetinib (A) or trametinib (B). Scale bar, 400 μm.

C-D. Representative images of Daoy tumorspheres following treatment with various concentrations of selumetinib (C) or trametinib (D). Scale bar, 400 μm.

Figure 8. Graphs depicting treatment with the MEK1/2 inhibitors significantly decreases tumorsphere size

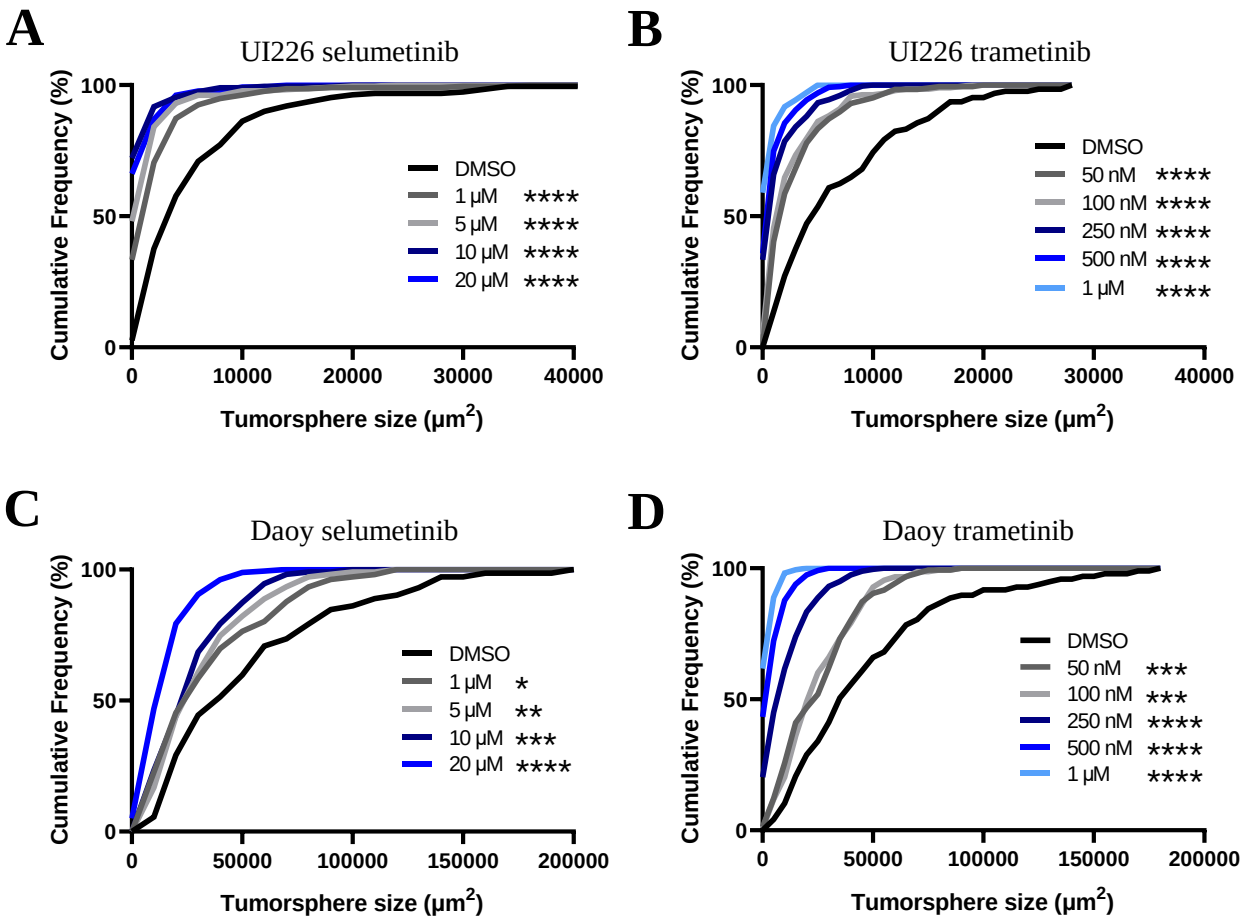

A-B. Quantification of UI226 tumorsphere size following treatment with increasing doses of selumetinib (A) or trametinib (B). Error bars, SEM. N=5 biological replicates and n=4 technical replicates for each biological replicate. Statistical analysis was completed using the Kolmogorov-Smirnov test. *, $P < 0.05$; **, $P < 0.01$; ***, $P < 0.001$; ****, $P < 0.0001$

C-D. Quantification of Daoy tumorsphere size following treatment with increasing doses of selumetinib (C) or trametinib (D). Error bars, SEM. N=6 biological replicates and n=4 technical replicates for each biological replicate. Statistical analysis was completed using the Kolmogorov-Smirnov test. *, $P < 0.05$; **, $P < 0.01$; ***, $P < 0.001$; ****, $P < 0.0001$

Figure 9. Treatment with the MEK1/2 inhibitors does not affect the total number of tumorspheres

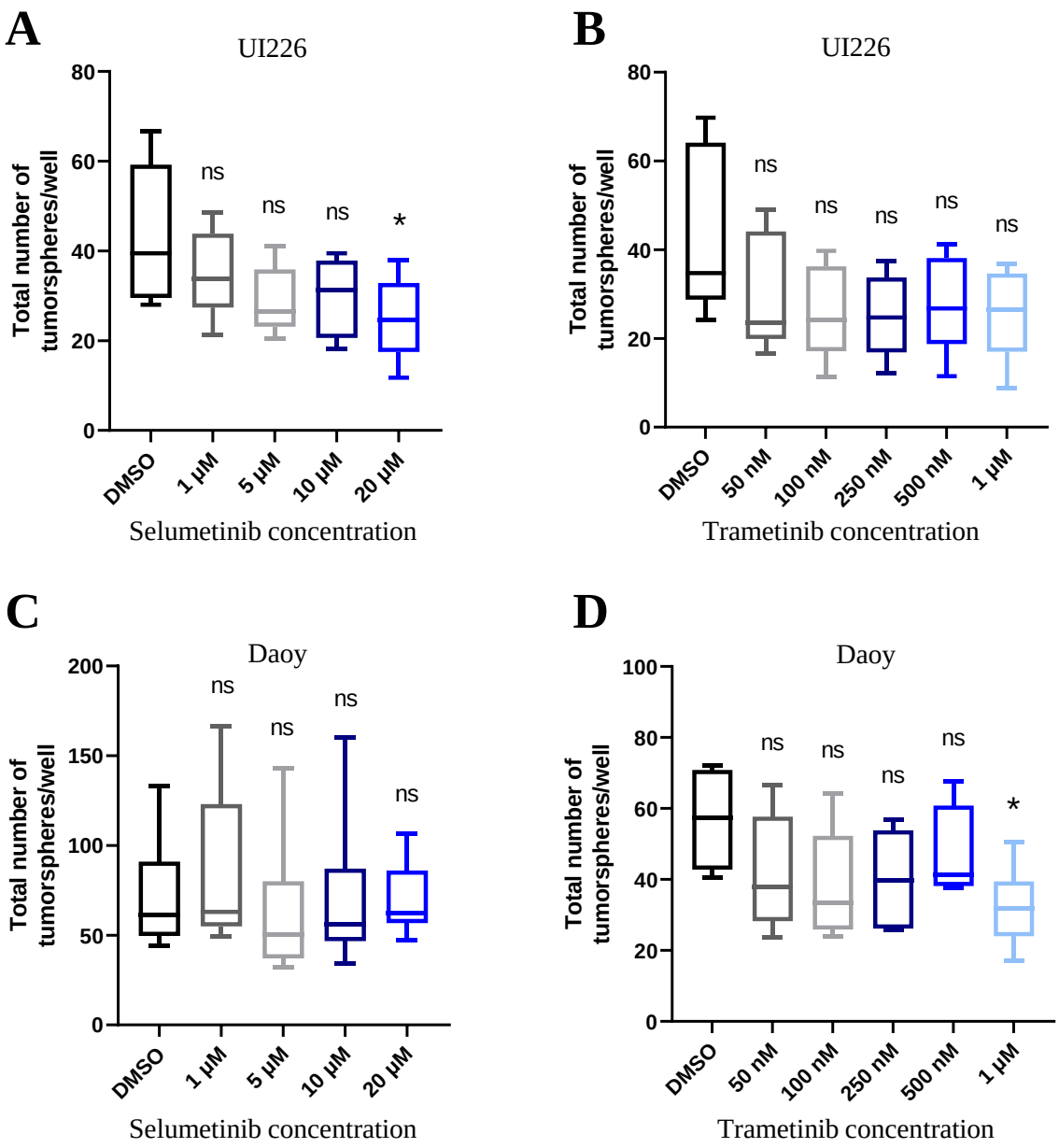

A-B) Quantification of UI226 tumorsphere number following treatment with increasing doses of selumetinib (A) or trametinib (B). Error bars, SEM. N=5 biological replicates and n=4 technical replicates for each biological replicate. Statistical analysis was completed using the Dunnett's multiple comparisons test. *, $P < 0.05$

C-D) Quantification of Daoy tumorsphere number following treatment with increasing doses of selumetinib (C) or trametinib (D). Error bars, SEM. N=6 biological replicates and n=4 technical replicates for each biological replicate. Statistical analysis was completed using the Dunnett's multiple comparisons test. *, $P < 0.05$

Figure 10. Treatment with the MEK1/2 inhibitors significantly decrease cell viability

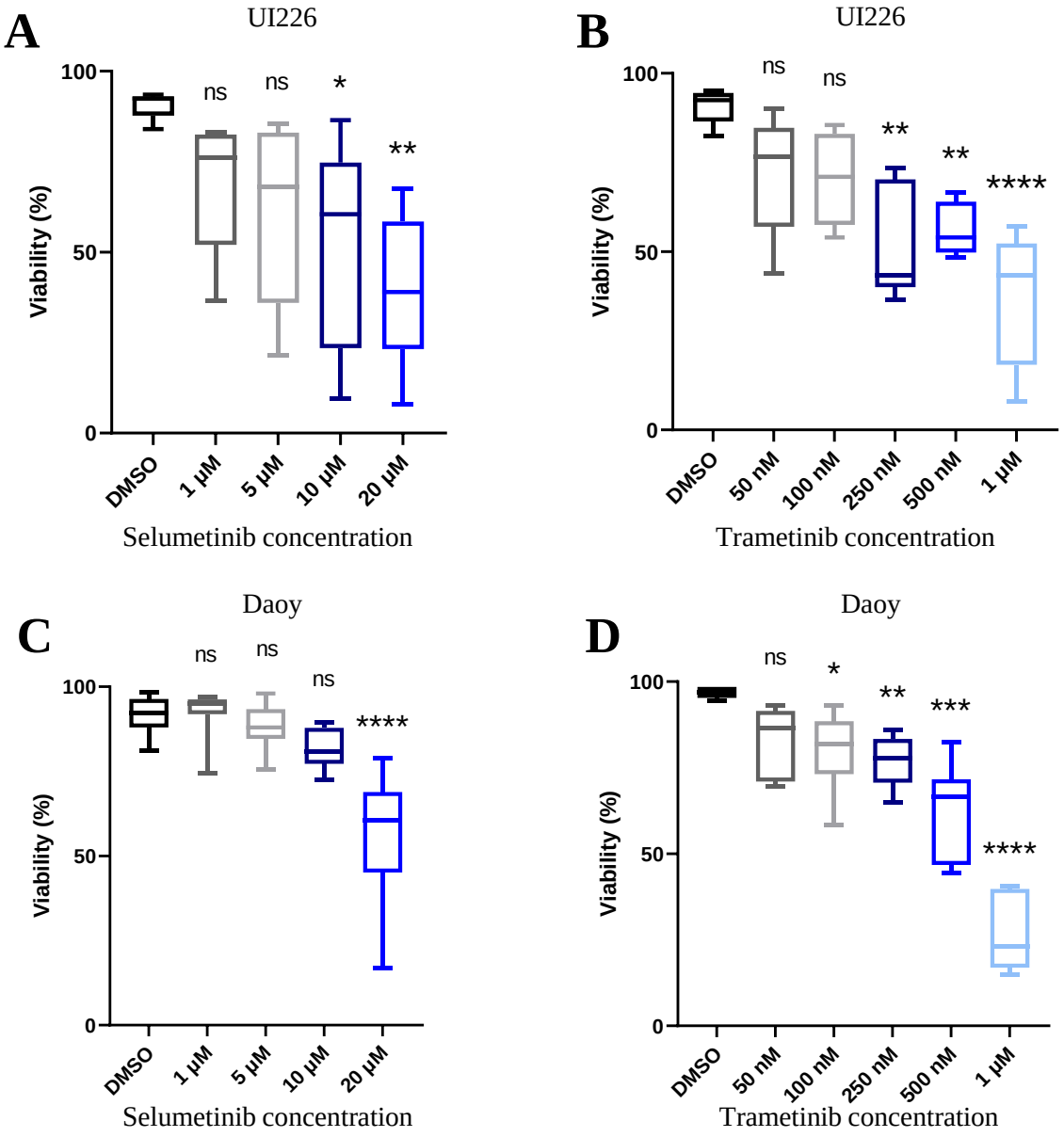

A-B) Quantification of UI226 cell viability following treatment with increasing doses of selumetinib (A) or trametinib (B). Error bars, SEM. N=5 biological replicates and n=4 technical replicates for each biological replicate. Statistical analysis was completed using the Dunnett's multiple comparisons test. *, $P < 0.05$; **, $P < 0.01$; ***, $P < 0.001$; ****, $P < 0.0001$

C-D) Quantification of Daoy cell viability following treatment with increasing doses of selumetinib (C) or trametinib (D). SEM. N=6 biological replicates and n=4 technical replicates for each biological replicate. Statistical analysis was completed using the Dunnett's multiple comparisons test. *, $P < 0.05$; **, $P < 0.01$; ***, $P < 0.001$; ****, $P < 0.0001$

Figure 11. Treatment with the MEK1/2 inhibitors significantly decreases cell migration

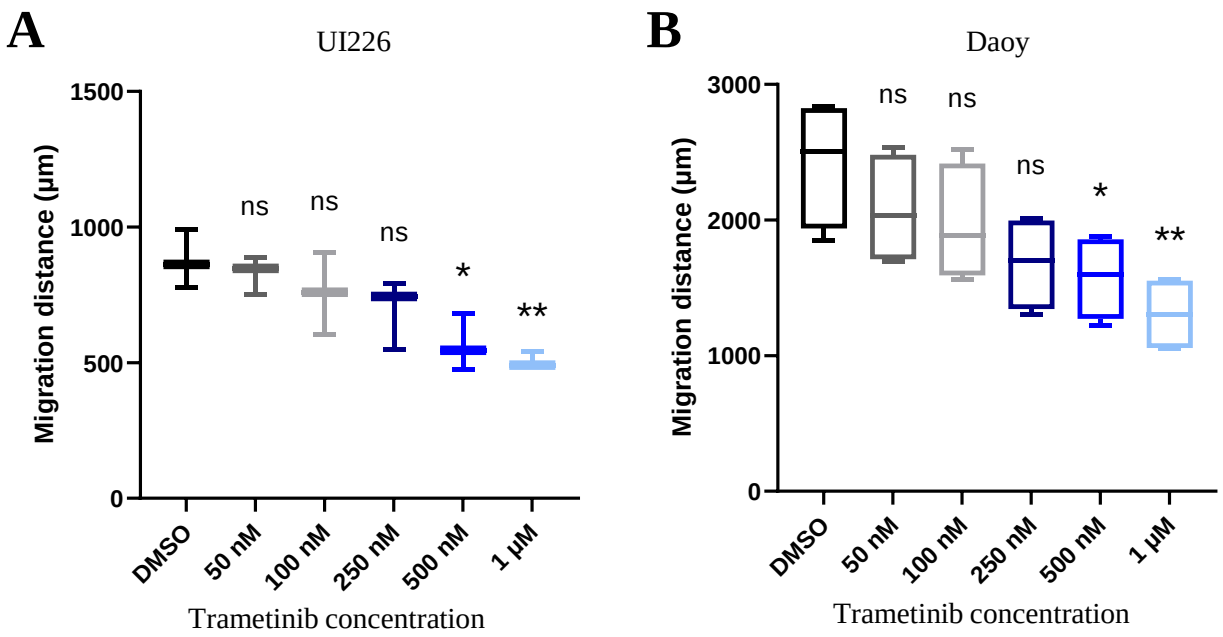

A-B) Quantification of cell migration following treatment with increasing doses of trametinib on UI226 cells (A) and Daoy cells (B). Error bars, SEM. N=3 biological replicates (UI226) and N=4 biological replicates (Daoy) and n=4 technical replicates for each biological replicate. Statistical analysis was completed using the Dunnett's multiple comparisons test. *, $P < 0.05$; **, $P < 0.01$

RNA sequencing reveals significant molecular changes in SHH MB tumorspheres following MEK inhibition.

To interrogate the molecular mechanisms associated with the decrease in tumor properties following trametinib treatment, we performed RNA sequencing (RNA-seq) on UI226 SHH MB tumorspheres to characterize the early (3 days) relative to the late or sustained (7 days) transcriptomic changes following trametinib treatment *in vitro.* Initial assessments of cell death in our tumorsphere assay revealed a significant decline at 250 nM trametinib treatment. Therefore, this concentration was chosen for RNA seq analyses. Comparison of day 3 and day 7 treated tumorspheres revealed significant overlap between the timepoints (**Fig. 12**). Of the 6499 significantly differentially expressed genes (padj <0.05) following 3 days trametinib treatment, 76% (4938 genes) were similarly up (2242 genes) or downregulated (2696) at day 7 (**Fig. 12**). Hallmark gene sets associated with E2F and myc targets as well as G2M checkpoint and neural stem cells were among the most significantly enriched downregulated gene sets following trametinib treatment at both timepoints (**Fig. 13 and 14A-D**). These results provide support for our *in vitro* assays demonstrating growth-related inhibitory effects on our stem cell enriched tumorsphere populations. The differences observed at day 3 were only further enhanced at day 7 (**Fig. 15A-D**). Additionally, we also observed that genes associated with SHH-stimulated granule neuron progenitor cell proliferation were enriched in gene sets that were downregulated following 7 days of trametinib treatment (**Fig. 16A-B**). In contrast, genes associated with astrocytic differentiation and ciliopathies were significantly enriched in gene sets that were upregulated at day 7 (**Fig. 16C-F**) suggesting an overall shift in cell fate decisions. This is interesting, as ciliopathies are disorders of the cerebellum that are caused by mutations in ciliary genes which leads to aberrant SHH signaling. Primary cilia are crucial for normal SHH signaling during human

brain development[75,76]. Defects in ciliary genes affects SHH signaling dependent proliferation of GNPC in the cerebellum which can result in SHH MB. Collectively, the transcriptomic changes following trametinib treatment demonstrate significant and sustained alterations in cell cycle and differentiation pathways.

Figure 12. Differentially expressed genes in day 3 and day 7 trametinib vs DMSO

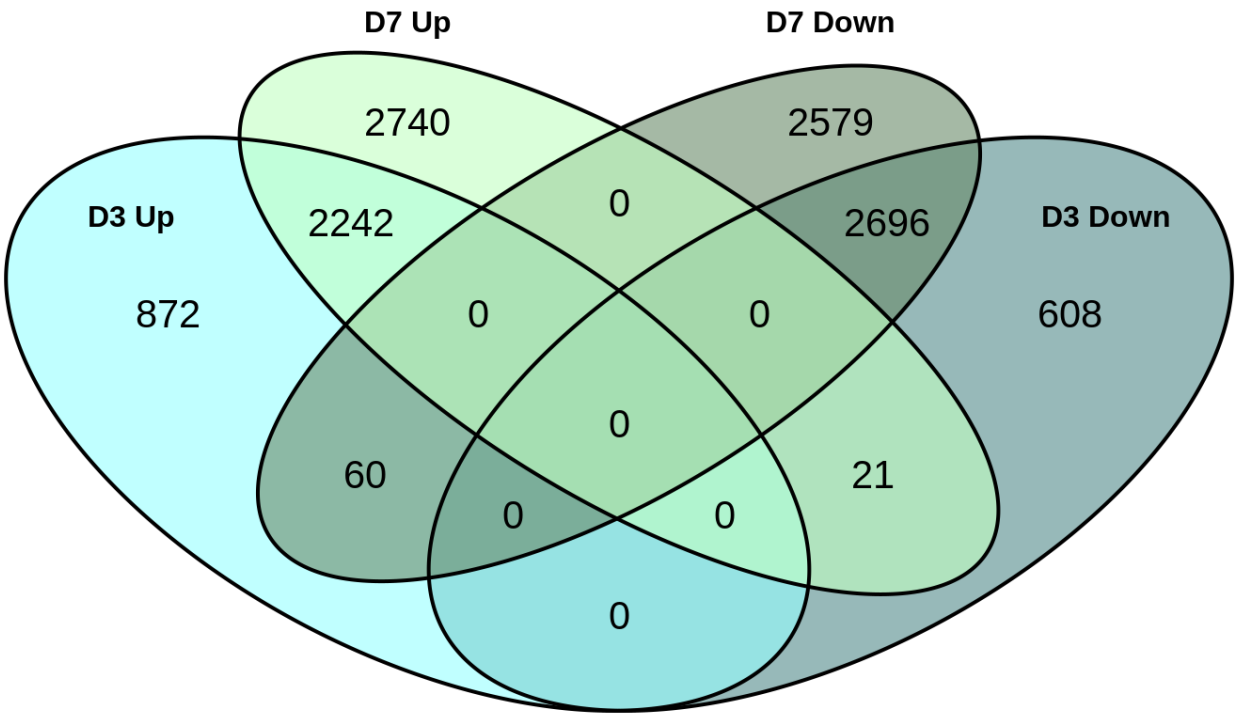

RNA sequencing was performed on UI226 SHH MB tumorspheres to characterize the sustained transcriptomic changes 3 days and 7 days following trametinib treatment *in vitro.* This Venn diagram is showing the number of genes that are altered that are unique to one time frame and the number that overlap between both 3 days and 7 days.

Figure 13. MEK inhibition significantly alters the transcriptome of UI226 SHH MB treated tumorspheres.

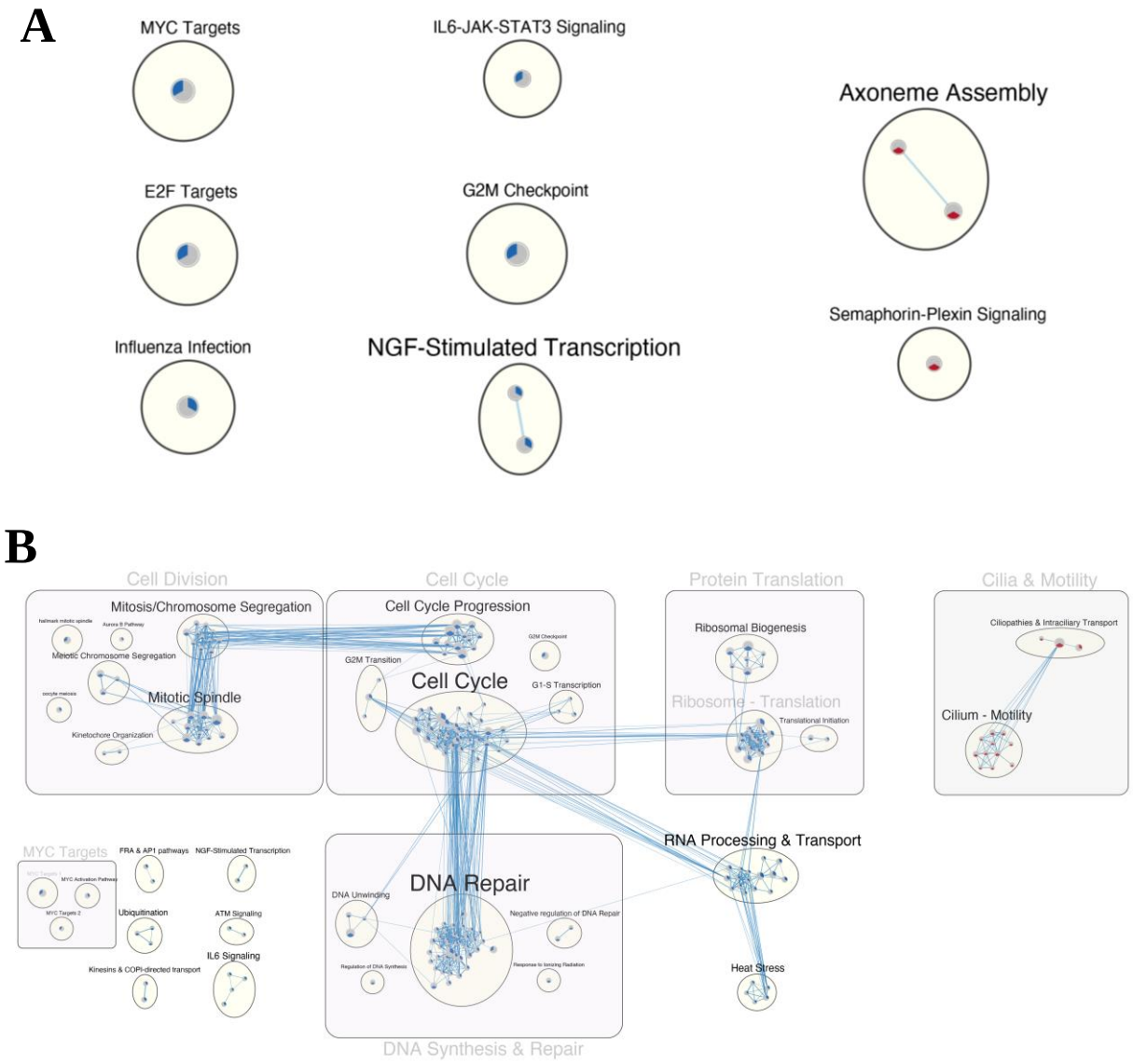

A-B. Enriched pathways and biological processes as determined by GSEA following 3 days (a) or 7 days (b) trametinib treatment of UI226 tumorspheres. GSEA results for Hallmark, Canonical Pathways (C2:CP), and Gene Ontology (C5) (q-value <0.01) were used to build the enrichment map. Node colouring is based on the normalized enrichment score (NES), with blue representing enrichment in vehicle and red representing enrichment in trametinib samples.

Figure 14. GSEA depicting gene sets significantly enriched (p<0.05) in genes that are downregulated following 7 days of trametinib treated UI226 SHH MB tumorspheres

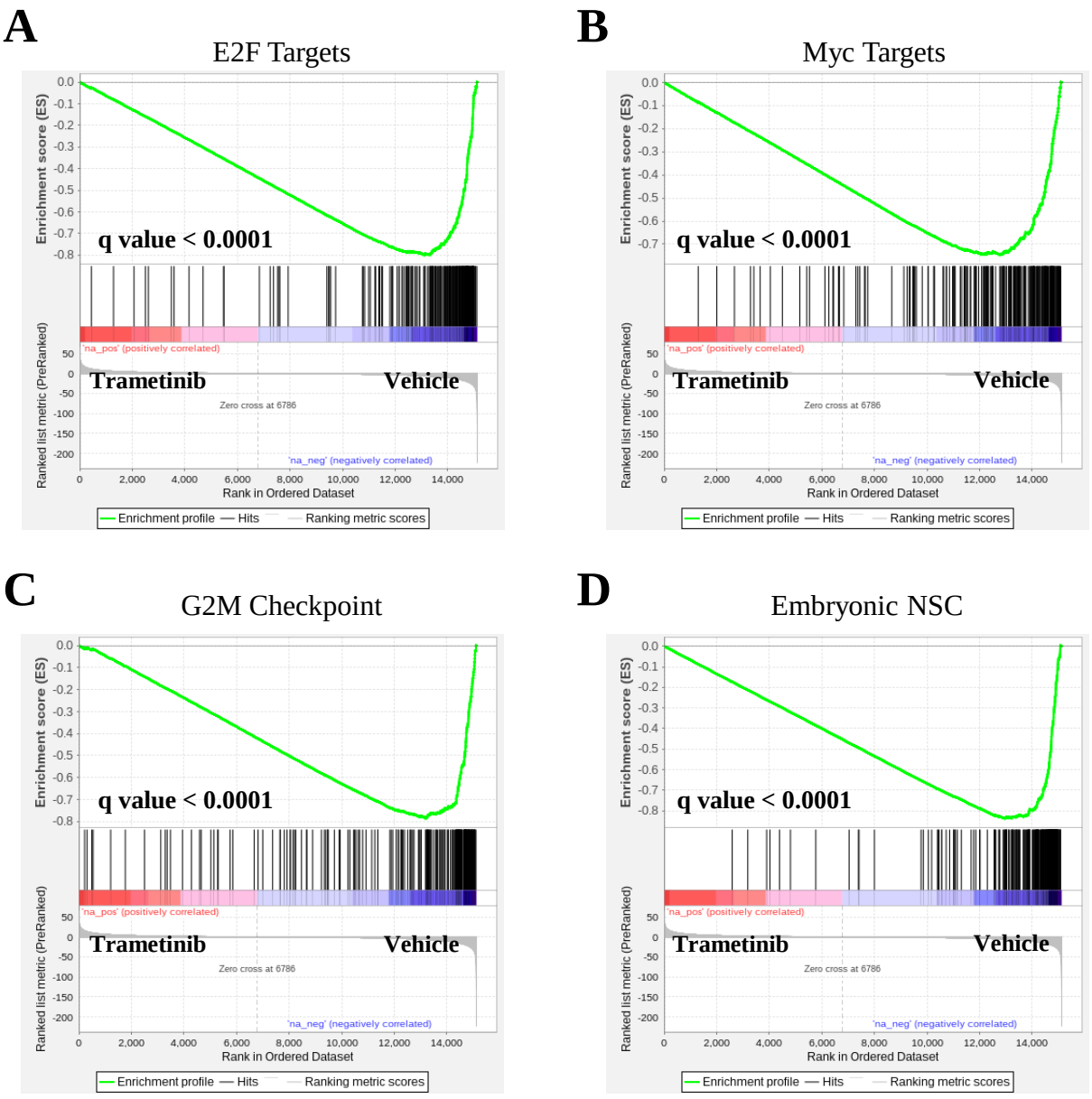

A-D. GSEA depicting gene sets associated with E2F targets (A), Myc targets (B), G2M checkpoint (C), and embryonic cortex neural stem cell markers (D) are enriched in genes sets that are downregulated following 7 days of trametinib treatment in UI226 SHH MB tumorspheres. padj<0.0001**** for all signatures.

Figure 15. Heat maps depicting gene sets that are downregulated following 3 days and 7 days of trametinib treated UI226 SHH MB tumorspheres

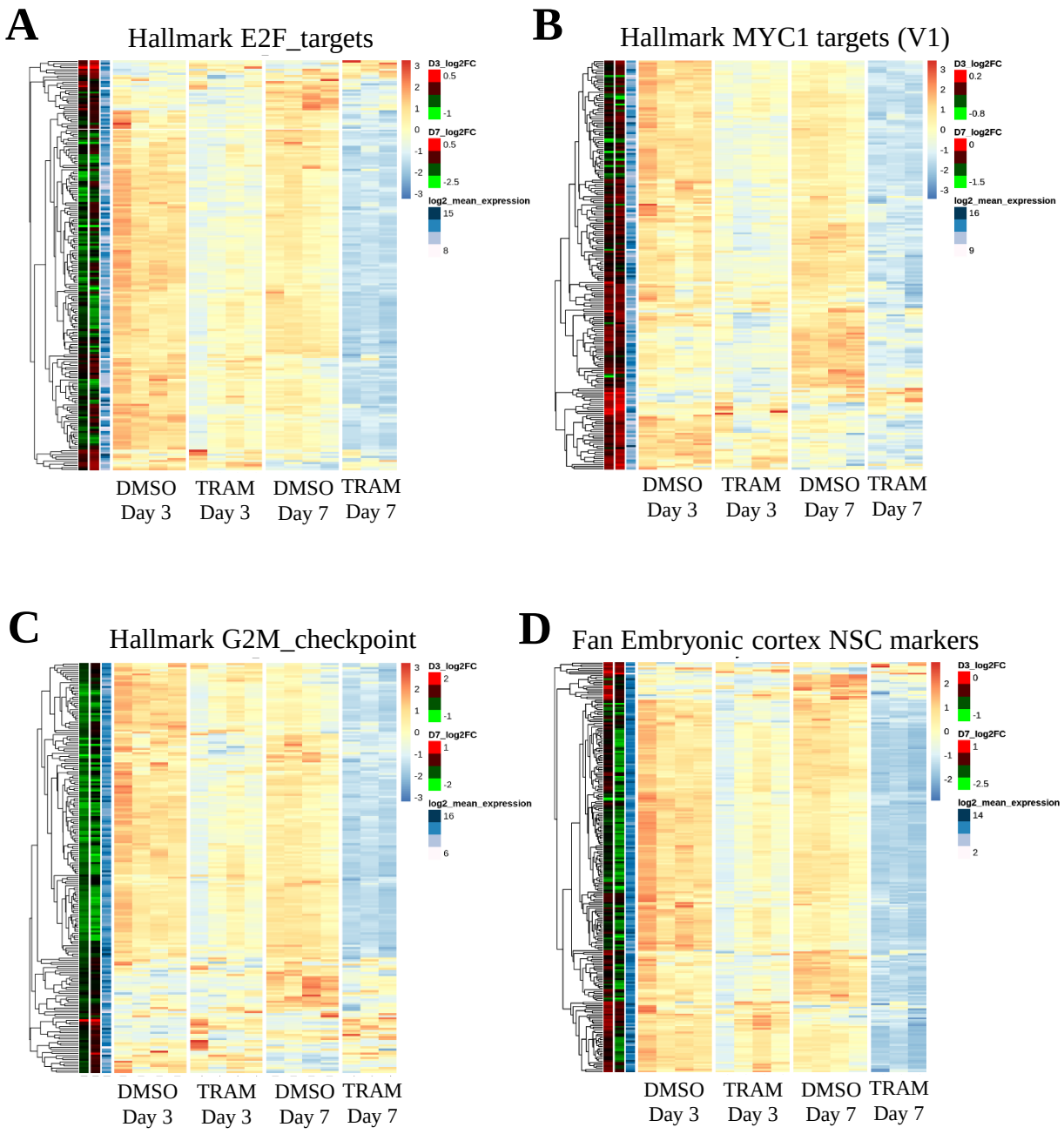

A-D. Heat maps depicting gene sets associated with E2F targets (A), Myc targets (B), G2M checkpoint (C), and embryonic cortex neural stem cell markers (D) are enriched in genes sets that are downregulated following trametinib treatment at day 3 that were only further enhanced at day 7. Red colour corresponds with upregulation and blue colour corresponds with downregulation.

Figure 16. GSEA and heat maps depicting gene sets that are downregulated or upregulated following 7 days of trametinib treated UI226 SHH MB tumorspheres

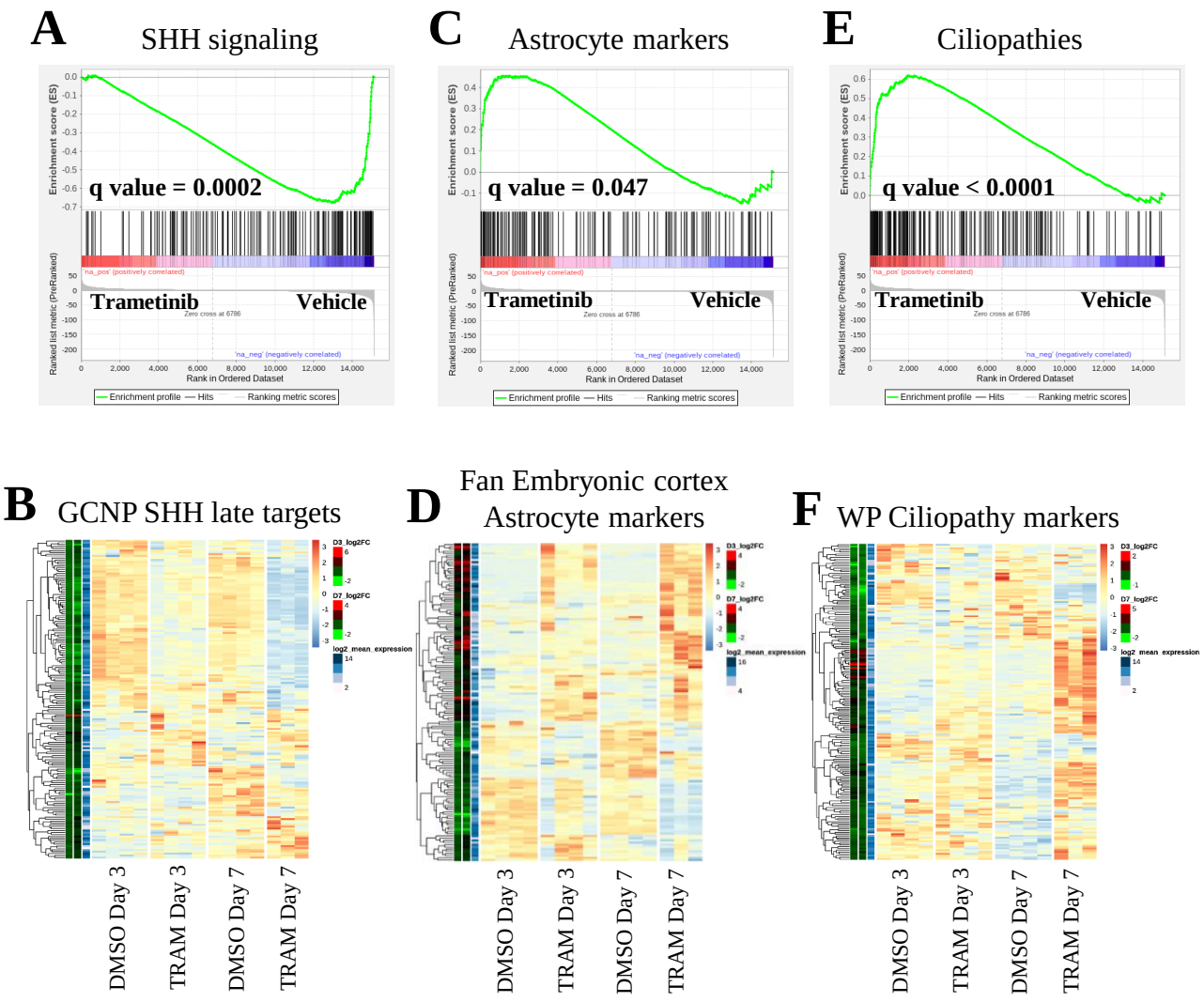

A-B. GSEA (A) and heat map (B) depicting gene sets associated with SHH signaling are enriched in genes sets that are downregulated following 7 days of trametinib treatment. padj<0.05* for all signatures. Red colour corresponds with upregulation and blue colour corresponds with downregulation.

C-F. GSEA (C and E) and heat maps (D and F) depicting gene sets associated with embryonic cortex astrocyte markers (C-D) and ciliopathies (E-F) are enriched in genes sets that are upregulated following 7 days of trametinib treatment. padj<0.05* for all signatures. Red colour corresponds with upregulation and blue colour corresponds with downregulation.

MEK1/2 inhibition significantly increases survival and reduces tumor growth in MB xenograft models.

Trametinib significantly decreases tumorigenic properties of SHH MB cells *in vitro* and is also known to be blood brain barrier penetrant[115]. We therefore tested the effect of this potent MEKi in xenograft mouse models (**Fig. 17**). First, immunohistochemistry (IHC) was performed on formalin-fixed paraffin-embedded (FFPE) tissue sections derived from control tumors from 3 MB xenograft models to determine potential efficacy *in vivo.* This includes our UI226 SHH MB model and the recently derived RCMB18 SHH MB PDX model that exhibits loss of *TP53, MYCN* amplification and a *SMO* mutation[66,95]. We also evaluated HDMB03 Group 3 MB xenografts to determine subgroup specificity and potential responsiveness in a model of the most highly aggressive MB. Three tumors from each MB model were stained with an anti-mitochondria antibody to specifically visualize human cells in NOD SCID mice (**Fig. 18A**). Sister sections from each xenograft model were then stained for p-ERK (**Fig. 18B**). Interestingly, UI226 SHH MB tumor cells were all strongly positive for p-ERK compared to RCMB18 SHH MB tumors which exhibited much lower positive p-ERK staining (**Fig. 18B**). Group 3 HDMB03 MB xenografts also exhibited lowers levels of p-ERK (**Fig. 18B**). These results suggest that the UI226 SHH MB xenograft model would be the most responsive to trametinib treatment *in vivo*.

Figure 17. Schematic outlining the xenograft mouse model experiments

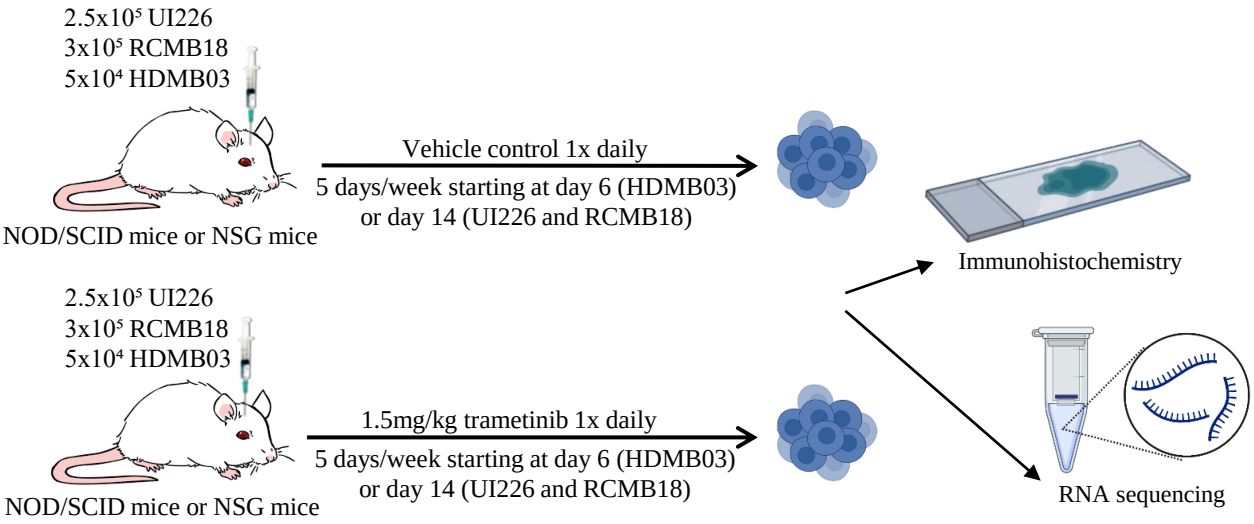

Schematic outlining the 3 xenograft mouse model experiments. $2.5x10^5$ cells/animal (UI226), $3x10^5$ cells/animal (RCMB18) or $5x10^4$ cells/animal (HDMB03) were injected into the cerebellum of immunodeficient NOD SCID or NSG mice. Vehicle control or 1.5mg/kg of trametinib was administered via oral gavage on a 5 day on, 2 day off schedule following tumor engraftment. Treatment started 6 days after tumor engraftment for the HDMB03 cells and 14 days after tumor engraftment for the UI226 and RCMB18 cells. When endpoint was reached, the animals were either perfused and their brains were extracted for immunohistochemical analysis, or their brains were removed and dissociated for RNA sequencing.

Figure 18. MAPK activity varies across MB cell models

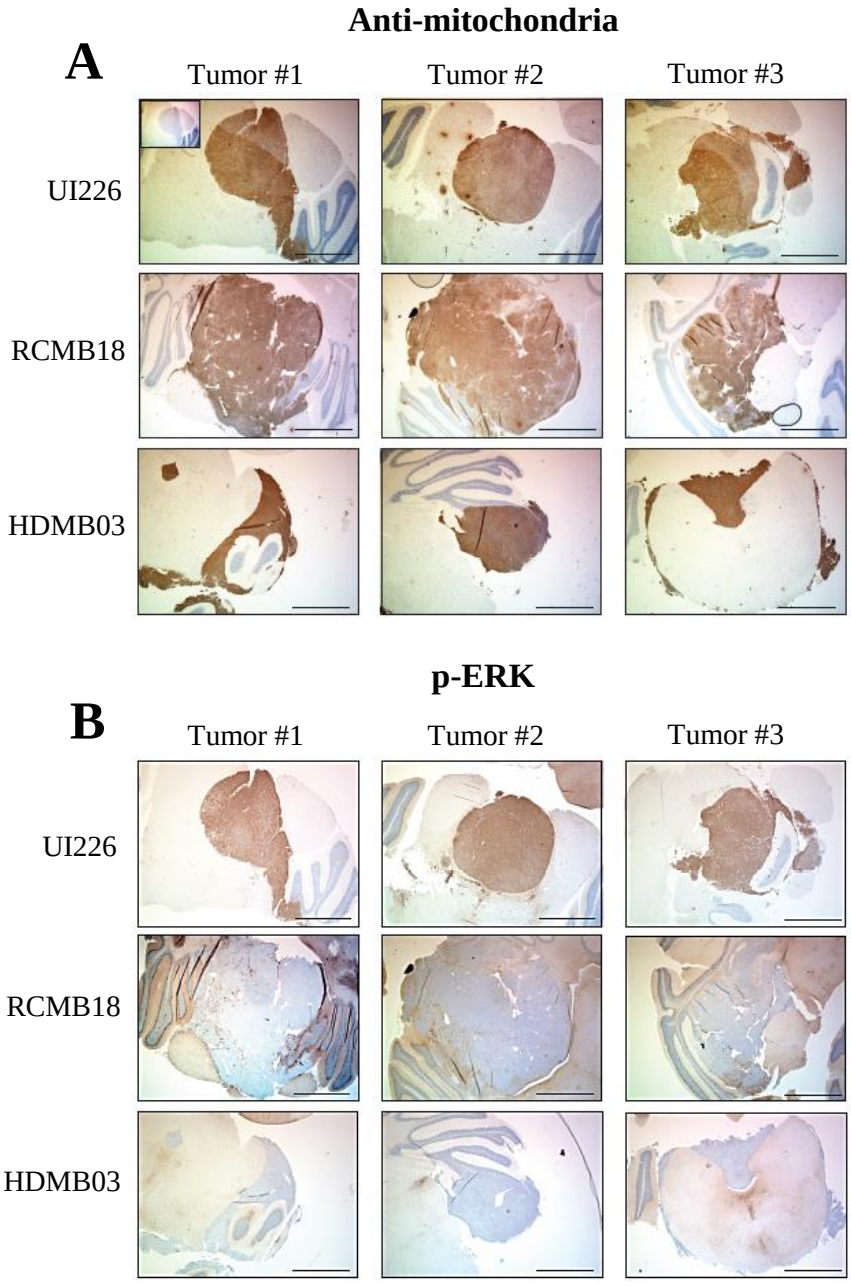

A-B. Representative images of immunohistochemical staining for anti-mitochondria antibody (A) and p-ERK antibody (B) in FFPE tissue sections derived from three representative independent control tumors from UI226 SHH MB, RCMB18 SHH MB and HDMB03 Group 3 MB xenograft models. Scale bars: 1550 μm.
*Completed by Ludivine Morrison

Next, a pilot study was completed to evaluate trametinib toxicity in NOD SCID mice without tumors using 0.5 mg/kg, 1.0 mg/kg, and 1.5 mg/kg. Gao et al.[127] recently evaluated the effect of trametinib on glioma xenograft models using one daily treatment with 1.0 mg/kg of trametinib. This study was used as the basis for the choice of concentrations in our models. At all 3 concentrations, the mice showed no signs of toxicity and consistently gained weight over 28 days of treatment (**Fig. 19**). Thus, we chose 1.5mg/kg of trametinib for further studies in all 3 xenograft models.

Figure 19. Trametinib is not toxic to NOD SCID mice

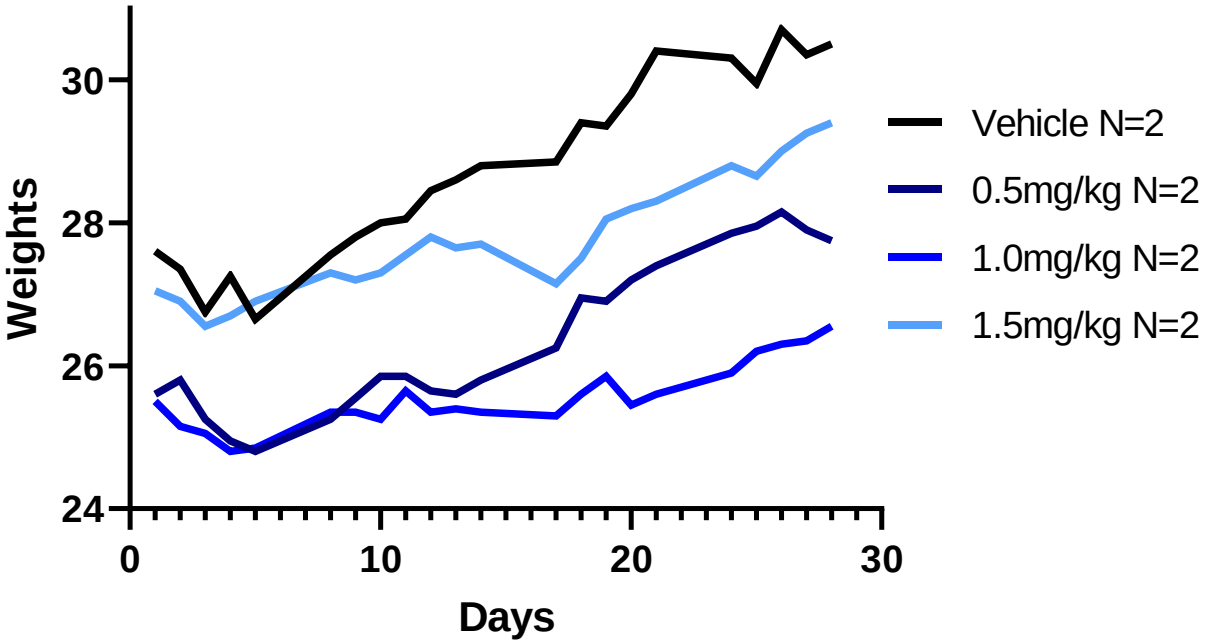

NOD SCID mice were administered vehicle or three different concentrations of trametinib to evaluate drug toxicity over 28 days. Each treatment group consisted of 2 mice that were administered 0.1 mL trametinib or vehicle control once daily via oral gavage on a 5 day on, 2 day off schedule. The vehicle control mice received MCPS80, the same liquid that drug is dissolved in. After 28 days the animals showed no signs of toxicity and continuously gained weight.

UI226 SHH MB tumorspheres ($2.5x10^5$ cells/animal), RCMB18 SHH MB PDX cells ($3x10^5$ cells/animal) and Group 3 MB HDMB03 cells ($5x10^4$ cells/animal) were injected into the cerebellum of immunodeficient NOD SCID or NSG mice. Trametinib was then administered, via oral gavage, on a 5-day on, 2-day off schedule until endpoint was reached. This "drug holiday" on weekends is associated with highly favorable toxicity profiles[114], and as anticipated, weights steadily increased overtime following trametinib treatment (**Fig. 20A-C**). MRI analysis of UI226 SHH MB tumors 66 days post-tumor cell injection revealed that the 6 remaining trametinib treated mice harbored tumors of varying size with 4 animals still exhibiting small tumors compared to the lone vehicle control which contained a very large tumor prior to endpoint (**Fig. 21A**). This translated to an overall significant increase in survival of UI226 SHH MB trametinib treated xenografts (**Fig. 21B**). RCMB18 SHH MB xenografts did not exhibit a significant increase in survival (**Fig. 21C**), likely attributed to their lower levels of MAPK activity (**Fig. 18B**). However, a trend towards increased survival was observed (median survival of 173 days in the trametinib group relative to 157 days in the vehicle controls). HDMB03 MB xenografts display similarly low levels of p-ERK; however, trametinib significantly extended survival in this highly aggressive Group 3 model (**Fig. 21D**). Collectively, these results support our *in vitro* studies and corroborate our IHC findings demonstrating robust MAPK activity particularly in the UI226 SHH MB xenografts. These results demonstrate the potential clinical utility of trametinib for treating MB tumors with elevated MAPK activity.

Figure 20. NOD SCID and NSG mouse weights during trametinib treatment indicating no signs of toxicity

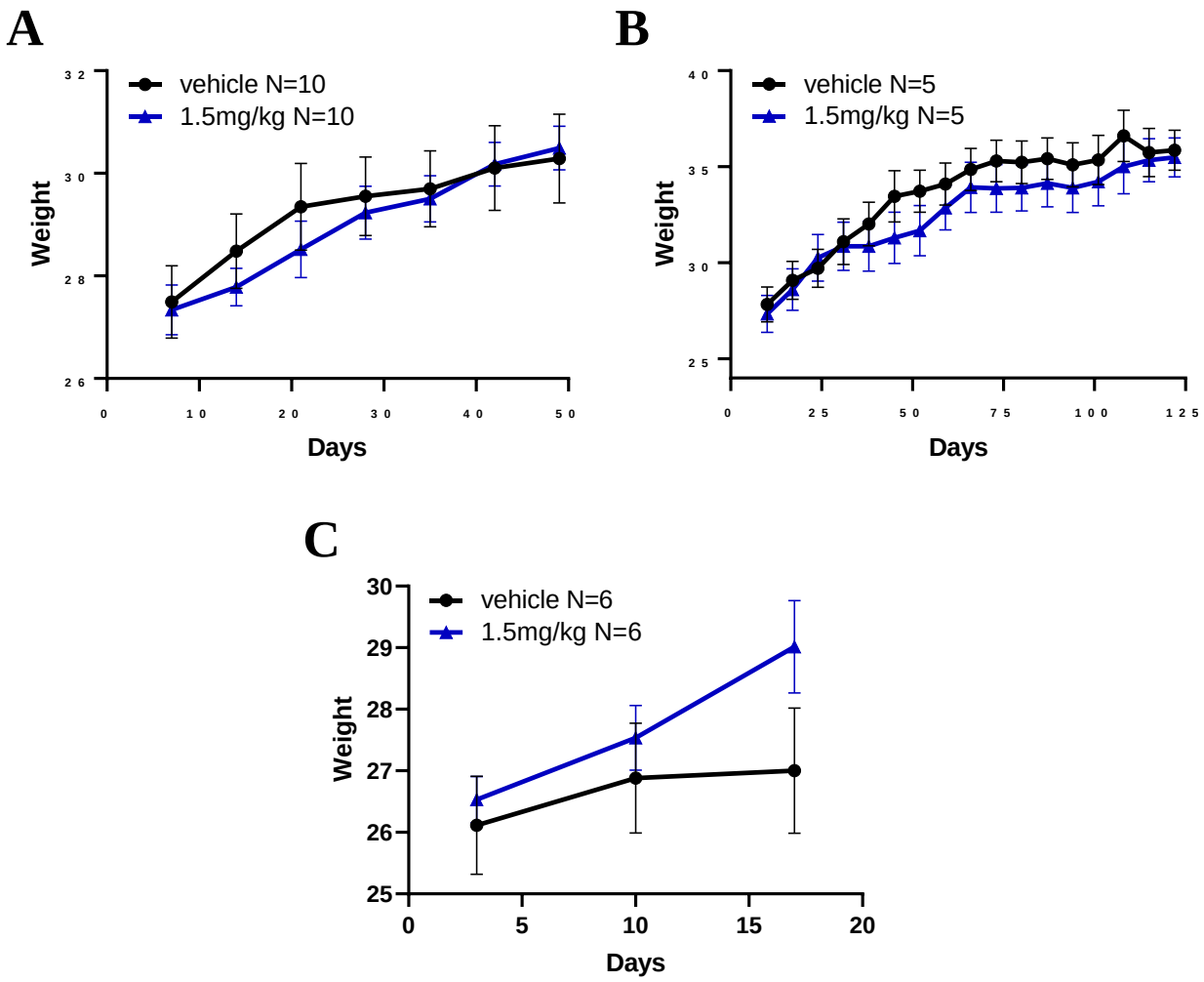

A-C. NOD SCID and NSG mouse weights over time following vehicle control (black) or 1.5mg/kg trametinib treatment (blue) post tumor engraftment with UI226 SHH MB cells (N=10) (A), RCMB18 SHH MB cells (N=5) (B) or HDMB03 Group 3 MB cells (N=6) (C). Drug treatment began at day 14 following injection of UI226 and RCMB18 tumor cells and at day 6 following injection of HDMB03 tumor cells. Error bars: SEM.

Figure 21. Trametinib treatment significantly extends survival in UI226 and HDMB03 tumors *in vivo*

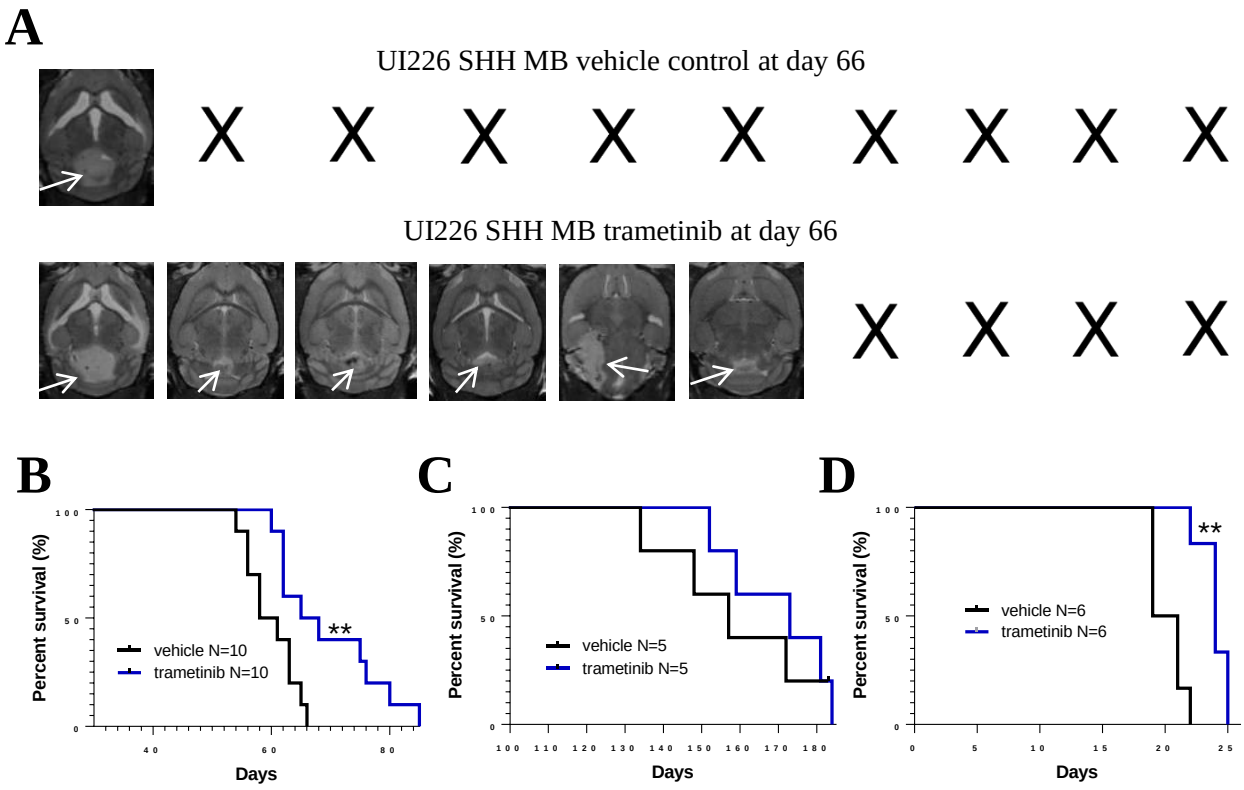

A. Representative MRI images of UI226 SHH MB tumors in NOD SCID mice treated with vehicle control or 1.5mg/kg trametinib at 66 days post surgery. One control out of 10 remained and 6 trametinib treated mice out of 10 remained.

B-D. Kaplan–Meier curves following transplantation of NOD SCID mice with $2.5x10^5$ UI226 SHH MB cells (N=10) (B), NSG mice with $3.0x10^5$ RCMB18 SHH MB cells (N=5) (C), and NOD SCID mice with $5.0x10^4$ HDMB03 Group 3 MB cells (N=6) (D). Mice were treated with vehicle control or 1.5 mg/kg of trametinib. p-value was determined using the log-rank test. **, $p<0.01$. Treatment started 14 days following UI226 and RCMB18 tumor cell injection and 6 days following HDMB03 tumor cell injection. Animals were treated once daily, 5 days a week by oral gavage, with a 2-day drug holiday on weekends until they reached endpoint.

Molecular pathways are differentially expressed following trametinib treatment *in vivo.*

Next, RNA sequencing was performed to interrogate the transcriptome changes following trametinib treatment in our responsive UI226 MB xenograft model. Endpoint tumors from UI226 SHH MB xenografts were extracted from trametinib treated mice (N=3) and vehicle controls (N=3). XenofilteR was performed to remove reads that mapped to the mouse genome (**Fig. 22**). In terms of individual gene expression, the vehicle and trametinib-treated tumors were similar at endpoint, as only 113 genes were significantly ($p<0.05$) differentially expressed (**Table 8**). However, in line with our tumorsphere data (**Fig. 14**), GSEA revealed that genes associated with E2F targets were enriched in genes sets that were significantly downregulated in trametinib-treated xenografts compared to vehicle controls (**Fig. 23A, Table 9**). Interestingly, genes associated with fatty acid metabolism and DNA repair were also enriched in significantly downregulated gene sets (**Fig. 23B-C**). Additionally, we also observed similar results to what was previously observed following selumetinib treatment *in vivo*[114]. Specifically, gene sets associated with oxidative phosphorylation are downregulated in trametinib treated xenografts compared to the vehicle controls (**Fig. 23D**) while genes associated with JAK/STAT3 signaling and TNFα/NFκB pathways are enriched for genes that are upregulated in trametinib treated xenografts (**Fig. 23E-F, Table 10**). These results demonstrate that trametinib inhibits cell cycle and DNA repair pathways following long term MEKi treatment. However, this is also accompanied by upregulation of cell signaling pathways that may be compensating for MEK inhibition *in vivo*.

Figure 22. SE Alignment scores

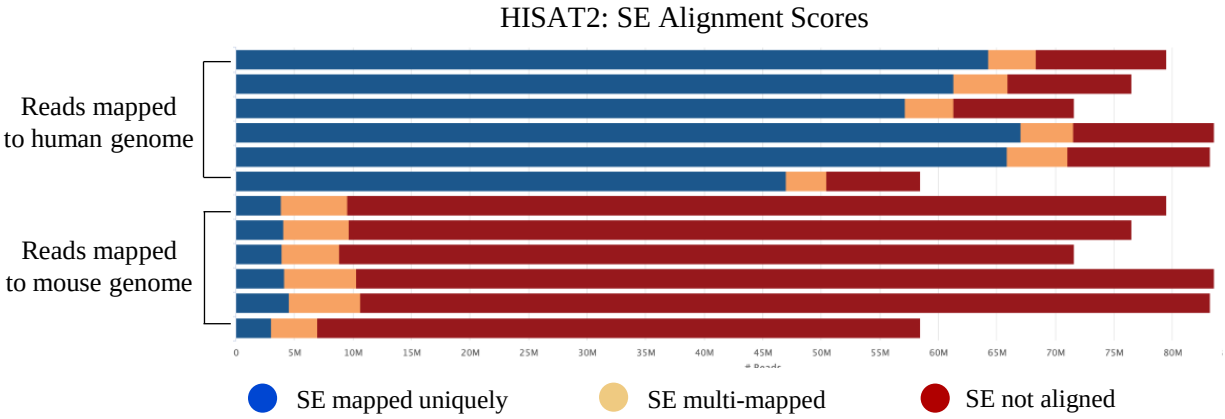

Reads were mapped to both human and mouse genomes and XenofilteR was then run to remove the reads that mapped better to mouse. There are between 58M and 84M reads per sample and the fraction of reads mapping to human is much greater than the fraction mapping to mouse.

Table 8: Genes significantly ($p<0.05$) and differentially expressed following trametinib treatment in UI226 SHH MB xenografts

hgnc_symbol	log2FoldChange	p-value	padj	ensembl_gene_id
RHEBP2	-7.8615	5.00E-07	0.0005	ENSG00000226964
SGCD	-3.0048	2.44E-06	0.0015	ENSG00000170624
LINC01036	-2.5870	1.06E-05	0.0045	ENSG00000230426
SPEGNB	-2.5743	7.69E-06	0.0037	ENSG00000286095
MAGEA1	-2.0403	1.25E-05	0.0050	ENSG00000198681
FBN3	-1.7882	1.10E-05	0.0045	ENSG00000142449
TMSB4XP1	-1.6032	5.93E-07	0.0005	ENSG00000236876
MECP2	-1.3369	5.30E-09	1.39E-05	ENSG00000169057
ABCA4	-1.2779	1.07E-05	0.0046	ENSG00000198691
RHCG	-1.2112	1.76E-07	0.0002	ENSG00000140519
AQP1	-1.0307	1.85E-05	0.0065	ENSG00000240583
RXRG	-1.0307	3.95E-05	0.0119	ENSG00000143171
NRK	-0.9554	6.37E-06	0.0033	ENSG00000123572
STEAP2	-0.8469	0.000240	0.0499	ENSG00000157214
NUF2	-0.8457	1.52E-05	0.0057	ENSG00000143228
FLVCR1-DT	-0.8330	0.000205	0.0439	ENSG00000198468
H4C15	-0.8082	2.39E-05	0.0079	ENSG00000270276
METTL7B	-0.8079	1.92E-07	0.0002	ENSG00000170439
ITGA7	-0.7299	0.000158	0.0361	ENSG00000135424
GPD1L	-0.7147	1.32E-08	2.58E-05	ENSG00000152642

BIRC5	-0.7060	8.37E-06	0.0039	ENSG00000089685
CHRDL1	-0.6570	2.41E-07	0.0002	ENSG00000101938
RADX	-0.6102	5.86E-06	0.0031	ENSG00000147231
CTNNBIP1	-0.5341	8.42E-05	0.0217	ENSG00000178585
PRKCI	-0.5277	0.0001	0.0295	ENSG00000163558
AGPAT5	-0.4799	1.95E-06	0.0013	ENSG00000155189
DSTYK	-0.4734	0.0002	0.0457	ENSG00000133059
KIAA1614	-0.4479	1.59E-05	0.0058	ENSG00000135835
TMCC2	-0.4281	6.90E-05	0.0184	ENSG00000133069
SMC4	-0.3948	2.92E-05	0.0094	ENSG00000113810
YIF1B	-0.3278	0.0001	0.0273	ENSG00000167645
TMSB4XP6	-0.0373	1.64E-07	0.0002	ENSG00000230043
SLITRK5	-0.0321	4.36E-05	0.0126	ENSG00000165300
PLA2G4A	-0.0300	4.97E-05	0.0139	ENSG00000116711
PRSS12	-0.0162	1.31E-05	0.0051	ENSG00000164099
SEPTIN14P2	-0.0136	1.62E-06	0.0011	ENSG00000244528
LINC01669	-0.0121	1.09E-05	0.0045	ENSG00000280191
FCRL2	-0.0112	2.30E-05	0.0078	ENSG00000132704
TAC4	-0.0110	8.13E-06	0.0039	ENSG00000176358
LINC01934	-0.0086	4.53E-05	0.0129	ENSG00000234663
CHRNA4	-0.0072	5.05E-05	0.0139	ENSG00000101204

GATM	0.4008	4.36E-05	0.0126	ENSG00000171766
SCD5	0.4109	1.76E-05	0.0063	ENSG00000145284
ANGPTL2	0.4414	1.63E-06	0.0011	ENSG00000136859
PMP22	0.4447	5.04E-06	0.0028	ENSG00000109099
PLAU	0.4544	0.0002	0.0439	ENSG00000122861
TFRC	0.4545	0.0001	0.0375	ENSG00000072274
PER3	0.4767	0.0002	0.0498	ENSG00000049246
ZHX3	0.4823	7.73E-05	0.0202	ENSG00000174306
SNCAIP	0.5145	4.49E-06	0.0026	ENSG00000064692
CREB5	0.5389	6.76E-07	0.0005	ENSG00000146592
HERC2P9	0.5611	4.87E-06	0.0027	ENSG00000206149
PHF21A	0.5702	9.41E-08	0.0001	ENSG00000135365
ZMIZ1	0.5723	6.55E-06	0.0033	ENSG00000108175
EMILIN3	0.5978	0.0001	0.0385	ENSG00000183798
FAM182A	0.6016	0.0002	0.0487	ENSG00000125804
LDB2	0.6360	2.30E-07	0.0002	ENSG00000169744
TNS2	0.7435	1.22E-06	0.0009	ENSG00000111077
KIF26B	0.7515	1.37E-06	0.0010	ENSG00000162849
PHKA2	0.7709	5.11E-08	8.57E-05	ENSG00000044446
DUSP1	0.8231	1.78E-05	0.0063	ENSG00000120129
MCM3AP	0.8388	4.96E-05	0.0139	ENSG00000160294

SCAMP1	0.8558	2.26E-09	7.59E-06	ENSG00000085365
SHD	0.8682	0.0002	0.0413	ENSG00000105251
CACNA1A	0.9105	0.0001	0.0349	ENSG00000141837
FLRT1	0.9788	0.0002	0.0360	ENSG00000126500
ARMH1	0.9913	0.0002	0.0358	ENSG00000198520
CACNG4	0.9917	1.24E-08	2.58E-05	ENSG00000075461
NDFIP2	0.9933	6.33E-05	0.0173	ENSG00000102471
LCMT1	0.9951	1.04E-09	4.07E-06	ENSG00000205629
SULF2	0.9960	0.0001	0.0307	ENSG00000196562
TGFB3	1.0061	8.89E-10	4.07E-06	ENSG00000119699
FXYD1	1.0066	3.87E-05	0.0118	ENSG00000266964
GTF2IP13	1.0276	6.16E-08	9.05E-05	ENSG00000272556
ATP6V1G2-DDX39B	1.0291	2.24E-08	4.05E-05	ENSG00000254870
RADIL	1.0545	0.0001	0.0279	ENSG00000157927
KLF4	1.2480	2.39E-13	1.87E-09	ENSG00000136826
TMEM135	1.2495	0.0002	0.0358	ENSG00000166575
IL6	1.2598	9.77E-06	0.0044	ENSG00000136244
RNF217	1.3031	3.13E-05	0.0097	ENSG00000146373
LINC02577	1.3553	0.0002	0.0370	ENSG00000228742
TMEM132B	1.3634	3.97E-06	0.0023	ENSG00000139364
BCLAF1P2	1.4179	2.91E-07	0.0003	ENSG00000279800

PSMC1P1	1.4675	7.76E-05	0.0202	ENSG00000241506
FOSB	1.5469	1.97E-05	0.0068	ENSG00000125740
SMAD1	1.6122	3.44E-05	0.0106	ENSG00000170365
TNR	1.7121	2.82E-09	8.27E-06	ENSG00000116147
TMCC1	1.7352	9.67E-05	0.0244	ENSG00000172765
NTRK3	1.8364	1.51E-05	0.0056	ENSG00000140538
MUC4	1.8628	4.71E-11	2.76E-07	ENSG00000145113
CSTF3-DT	2.9027	6.02E-08	9.05E-05	ENSG00000247151
LINC00649	3.0236	8.88E-09	2.09E-05	ENSG00000237945
HES2	3.1515	9.51E-05	0.0242	ENSG00000069812
RPL6P27	3.1869	3.61E-06	0.0022	ENSG00000235552
GOLGA6A	3.5124	8.94E-06	0.0041	ENSG00000159289
DGKG	3.6749	1.61E-107	3.77E-103	ENSG00000058866
HNRNPUP1	3.7398	0.0001	0.0292	ENSG00000259051
TNK2-AS1	4.6270	6.53E-05	0.0176	ENSG00000224614
IFI30	6.3776	1.49E-05	0.0056	ENSG00000216490
RAB6C	6.7148	4.17E-05	0.0123	ENSG00000222014
SPDYE2	7.4130	5.47E-06	0.0029	ENSG00000205238
RHEBP1	7.5381	2.25E-06	0.0014	ENSG00000229927
LINC02261	7.7005	1.07E-06	0.0008	ENSG00000249699
SEPTIN14P4	7.9331	3.04E-05	0.0096	ENSG00000251155

Figure 23. GSEA depicting gene sets that are downregulated or upregulated following trametinib treated UI226 SHH MB xenografts

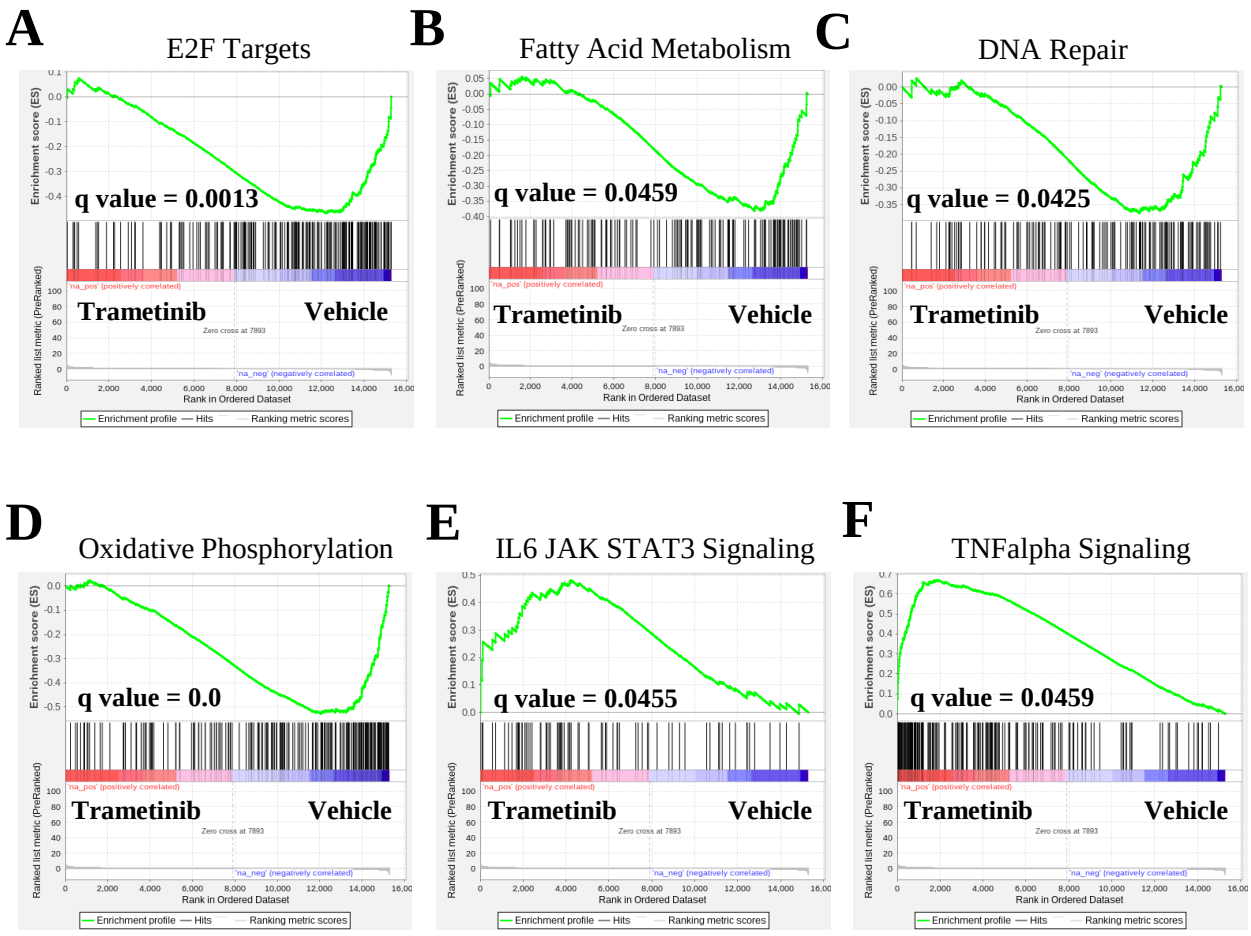

A-D. GSEA depicting genes associated with E2F targets (A), fatty acid metabolism (B), DNA repair (C) and oxidative phosphorylation (D) are enriched in genes sets that are downregulated following trametinib treatment. padj<0.05* for all signatures.

E-F. GSEA depicting genes associated with JAK/STAT3 signaling (E) and TNFalpha signaling (F) are enriched in genes sets that are upregulated following trametinib treatment. padj<0.05* for all signatures.

Table 9: Hallmark gene sets significantly enriched (p<0.05) in genes that are downregulated in trametinib treated UI226 SHH MB xenografts

NAME	SIZE	ES	NES	p-value	q-value
HALLMARK_OXIDATIVE_PHOSPHORYLATION	200	-0.5285	-2.1844	<0.0001	<0.0001
HALLMARK_E2F_TARGETS	197	-0.4683	-1.9209	<0.0001	0.0013
HALLMARK_ADIPOGENESIS	189	-0.3876	-1.6157	<0.0001	0.0203
HALLMARK_DNA_REPAIR	147	-0.3757	-1.4914	0.0034	0.0425
HALLMARK_FATTY_ACID_METABOLISM	143	-0.3813	-1.5136	0.0114	0.0459
HALLMARK_MYC_TARGETS_V1	200	-0.3259	-1.3361	0.0160	0.1293
HALLMARK_CHOLESTEROL_HOMEOSTASIS	69	-0.3668	-1.2892	0.0991	0.1368
HALLMARK_PEROXISOME	96	-0.3468	-1.3020	0.0686	0.1436
HALLMARK_G2M_CHECKPOINT	198	-0.3042	-1.2466	0.0416	0.1671
HALLMARK_XENOBIOTIC_METABOLISM	170	-0.2659	-1.0855	0.2334	0.4855
HALLMARK_SPERMATOGENESIS	98	-0.2761	-1.0399	0.3603	0.5878
HALLMARK_REACTIVE_OXYGEN_SPECIES_PATHWAY	47	-0.3012	-0.9914	0.4883	0.6522
HALLMARK_UNFOLDED_PROTEIN_RESPONSE	113	-0.2513	-0.9701	0.5415	0.6761
HALLMARK_BILE_ACID_METABOLISM	94	-0.2674	-0.9959	0.4668	0.6879
HALLMARK_GLYCOLYSIS	186	-0.2310	-0.9425	0.6250	0.7193

Table 10: Hallmark gene sets significantly enriched (p<0.05) in genes that are upregulated in trametinib treated UI226 SHH MB xenografts

NAME	SIZE	ES	NES	p-value	q-value
HALLMARK_IL6_JAK_STAT3_SIGNALING	73	0.4814	1.5320	0.0199	0.0455
HALLMARK_INFLAMMATORY_RESPONSE	150	0.4475	1.5905	0.0112	0.0456
HALLMARK_TNFA_SIGNALING_VIA_NFKB	183	0.6686	2.4293	<0.0001	0.0459
HALLMARK_WNT_BETA_CATENIN_ SIGNALING	39	0.5271	1.5326	0.0303	0.0493
HALLMARK_INTERFERON_GAMMA_ RESPONSE	185	0.4361	1.5940	0.0132	0.0499
HALLMARK_ESTROGEN_RESPONSE_EARLY	177	0.4456	1.6057	0.0188	0.0531
HALLMARK_COMPLEMENT	161	0.6469	2.2942	0.0013	0.0549
HALLMARK_EPITHELIAL_MESENCHYMAL_ TRANSITION	187	0.4411	1.6068	0.0131	0.0597
HALLMARK_HYPOXIA	189	0.4566	1.6584	0.0211	0.0630
HALLMARK_HEDGEHOG_SIGNALING	34	0.6028	1.7223	0.0066	0.0697
HALLMARK_P53_PATHWAY	183	0.3933	1.4147	0.0287	0.0726
HALLMARK_APOPTOSIS	149	0.4018	1.4163	0.0290	0.0771
HALLMARK_TGF_BETA_SIGNALING	54	0.6238	1.9046	0.0033	0.0793
HALLMARK_UV_RESPONSE_DN	139	0.6011	2.1525	0.0054	0.0810
HALLMARK_INTERFERON_ALPHA_RESPONSE	95	0.6080	2.0373	0.0107	0.0897

Chapter IV: Discussion

Current personalized therapies for SHH MB are lacking and novel, targeted therapies that have the potential to reduce toxicity and improve survival are urgently needed. Targeting MB tumor cells through MEK inhibition represents a novel and rational therapeutic strategy for the treatment of SHH MB. Liang et al. previously evaluated the effect of the MEKi selumetinib on SHH MB tumorigenic properties both *in vitro* and *in vivo*[106]. However, to our knowledge the more potent MEKi trametinib has not yet been tested in human SHH MB models. Trametinib is currently in clinical trials for the treatment of refractory low-grade gliomas and plexiform neurofibromas and has been approved for the treatment of adult BRAF V600E mutant cancers[115,116]. Trametinib crosses the blood brain barrier and is an FDA approved drug that could therefore potentially be available as a treatment option in human clinical trials of SHH MB. Our results show that the more potent MEKi trametinib significantly inhibits SHH MB tumor properties both *in vitro* and *in vivo*. Treatment with this MEKi had a significant effect on cell proliferation, viability, survival, and migration *in vitro* while also significantly increasing survival in 2 different MB xenograft mouse models *in vivo*. Together, these results warrant further investigation of trametinib as a novel therapeutic strategy for MB either as a single agent or in combination with other targeted therapies.

We recently identified molecular pathways that could be compensating for selumetinib treatment, thus contributing to molecular adaptation and drug resistance *in vivo*[114]. JAK/STAT3 pathway activation is upregulated in SHH MB tumor cells following treatment with selumetinib. Importantly, we showed that combined MEK and JAK/STAT3 pathway inhibition effectively decreases SHH MB tumor progression in cultures derived from 3 SHH MB models, as well as 2 SHH MB xenograft models. As we also observed enrichment of genes associated with

JAK/STAT3 signaling in trametinib treated xenografts, future studies will evaluate the effect of dual JAK/STAT3 pathway inhibition and trametinib on tumorigenic properties both *in vitro* and *in vivo.* Additionally, gene sets associated with TNFα/NFκB pathways were enriched for genes that are upregulated in trametinib treated xenografts. Therefore, future studies could also evaluate the effect of trametinib in combination with a TNFα/NFκB pathway inhibitor on tumorigenic properties. Finally, the combination of trametinib with other standard of care chemotherapeutic agents such as cisplatin or vincristine will also be explored.

Immunohistochemistry staining of tissue sections derived from different MB xenografts revealed variable p-ERK levels and therefore MAPK signaling activity across models. UI226 SHH MB tumors exhibited universally high p-ERK levels compared to the RCMB18 SHH MB and HDMB03 Group 3 tumors. The *in vivo* results supported these findings, as the most significant increase in survival was observed in the UI226 SHH MB xenografts following trametinib treatment. Surprisingly, a significant survival increase was also observed in the HDMB03 Group 3 xenograft model following trametinib treatment. While there was also a modest improvement in RCMB18 SHH MB survival, the increase was not significant. This could be attributed to molecular adaptation over the very long course of tumor progression in this model combined with the overall lower MAPK pathway activity. Future studies will evaluate the effect of a higher dose of trametinib in RCMB18 to identify the maximum tolerated dose of trametinib in xenograft models.

Additionally, our lab has previously identified novel roles for the CD271 cell marker in contributing to SHH MB growth and tumor progression[4,106]. Bioinformatics analyses of large patient datasets and tumorspheres from SHH MB cultures demonstrated that CD271 is a novel and

promising diagnostic marker for these tumors[106]. Moreover, we determined that genes enriched in the MAPK pathway were highly overexpressed in samples harbouring high CD271 levels. These cells were therefore responsive to selumetinib treatment both *in vitro* and *in vivo*[106]. CD271 is also known as the p75 neurotrophin receptor (p75NTR) or additionally as the nerve growth factor receptor (NGFR). This receptor is a transmembrane glycoprotein that plays a variety of roles in normal neurodevelopment including axon guidance, growth cone elongation, cell death and survival. Activation of this receptor through the JNK pathway appears to play a role in CD271 mediated cell death, whereas signaling through the NFκB pathway promotes survival. Our lab is therefore interested in pursuing CD271-mediated signaling along with the MAPK pathway to evaluate the effects of directly targeting the CD271 receptor and indirectly targeting these CD271+ cells through their association with the MEK/ERK pathway. We have extensively evaluated the indirect affects through MEK inhibition[106,114] however, a recent study has characterized a small molecule, NSC49652 that targets the transmembrane domain of CD271[128]. This drug kills CD271+ cells by triggering apoptotic cell death through the receptor and the JNK kinase pathway downstream. Additional studies will pursue novel drugs, such as NSC49652, that directly target the CD271 receptor to evaluate the effect of CD271/p75NTR inhibition on SHH MB tumor progression. We will determine whether this inhibitor can be used alone or in combination with other signaling pathway antagonists such as selumetinib or trametinib to treat SHH MB.

Previous studies have demonstrated that primary cilia are essential for SHH signaling during human brain development[75,76]. Our RNA seq data on trametinib treated tumorspheres revealed that genes associated with SHH-stimulated granule neuron progenitor cell (GNPC) proliferation were enriched in gene sets that were downregulated following 7 days of trametinib

treatment. The SHH signaling pathway plays an important role in the proliferation of GNPC in the external granular layer of the cerebellum during normal development and is thought to drive SHH MB tumorgenesis[13]. In contrast, genes sets associated with ciliopathies were the most significantly enriched gene sets that were upregulated following 7 days of trametinib treatment. This is interesting, as it is well known that primary cilium and SHH signaling are required for GNPC proliferation in the external granular layer of the cerebellum and that defects in either ciliary genes or mutations in SHH pathway genes can result in ciliopathies and contribute to SHH MB [75]. Ciliated MB tumors with SHH signaling could be susceptible to therapeutics that directly target primary cilia[75]. Understanding the role of primary cilia in normal and oncogenic signaling could lead to new insights into the mechanisms of tumorigenesis and provide rational for new treatment options for SHH MB.

Chapter V: Conclusion

Our study reveals a novel role for trametinib in effectively attenuating SHH MB tumor progression and supports the potential clinical utility of this potent MEKi to treat MB tumors with elevated MAPK pathway activity. Trametinib either alone or in combination with other upregulated signaling pathway inhibitors or chemotherapeutic agents could be translated into clinical trial development to generate new and innovative targeted therapies to treat these very aggressive pediatric brain tumors. This thesis provides the framework that will be used to identify new treatment options for SHH MB that will reduce toxicity, improve quality of life, and increase survival for future patients.

Cited Literature

1. Canadian Cancer Statistics 2019. (Canadian Cancer Society, Toronto, Ontario, 2019).
2. Hovestadt, V. *et al.* Medulloblastomics revisited: biological and clinical insights from thousands of patients. *Nat Rev Cancer* **20**, 42-56 (2020).
3. Packer, R.J., Cogen, P., Vezina, G. & Rorke, L.B. Medulloblastoma: clinical and biologic aspects. *Neuro Oncol* **1**, 232-50 (1999).
4. Lisa Liang, C.A., Kathleen Felton, Amanda Hogg, Frank van Landeghem, T. Klonisch, David D. Eisenstat and Tamra E. Werbowetski-Ogilvie. Primary Pediatric Brain Tumors of the Posterior Fossa Part II: A Comprehensive Overview of Medulloblastoma. in *Development of the Cerebellum from Molecular Aspects to Diseases* (ed. Marzban, H.) 327–351 (Springer, Cham, Springer, Cham, 2017).
5. *WHO Classification of Tumours Editorial Board. World Health Organization Classification of Tumours of the Central Nervous System, 5th Edition*, (2021).
6. Coluccia, D., Figuereido, C., Isik, S., Smith, C. & Rutka, J.T. Medulloblastoma: Tumor Biology and Relevance to Treatment and Prognosis Paradigm. *Curr Neurol Neurosci Rep* **16**, 43 (2016).
7. Park, T.S., Hoffman, H.J., Hendrick, E.B., Humphreys, R.P. & Becker, L.E. Medulloblastoma: clinical presentation and management. Experience at the hospital for sick children, toronto, 1950-1980. *J Neurosurg* **58**, 543-52 (1983).
8. Ramaswamy, V. *et al.* Risk stratification of childhood medulloblastoma in the molecular era: the current consensus. *Acta Neuropathol* **131**, 821-31 (2016).
9. Lannering, B. *et al.* Hyperfractionated versus conventional radiotherapy followed by chemotherapy in standard-risk medulloblastoma: results from the randomized multicenter HIT-SIOP PNET 4 trial. *J Clin Oncol* **30**, 3187-93 (2012).
10. Lafay-Cousin, L. *et al.* Clinical, Pathological, and Molecular Characterization of Infant Medulloblastomas Treated with Sequential High-Dose Chemotherapy. *Pediatr Blood Cancer* **63**, 1527-34 (2016).
11. Mehta, M., Chang S., Newton H., Guha A. & M., V. *Principles and Practice of Neuro-oncology: A multidisciplinary approach*, 951 (Demos Medical Publishing; 1 edition (Oct 21 2010), 2011).
12. Louis, D.N. *et al.* The 2007 WHO classification of tumours of the central nervous system. *Acta Neuropathol* **114**, 97-109 (2007).
13. Taylor, M.D. *et al.* Molecular subgroups of medulloblastoma: the current consensus. *Acta Neuropathologica* **123**, 465-72 (2012).
14. Crawford, J.R., MacDonald, T.J. & Packer, R.J. Medulloblastoma in childhood: new biological advances. *The Lancet Neurology* **6**, 1073-1085 (2007).
15. Ellison, D.W. *et al.* beta-Catenin status predicts a favorable outcome in childhood medulloblastoma: the United Kingdom Children's Cancer Study Group Brain Tumour Committee. *J Clin Oncol* **23**, 7951-7 (2005).
16. Ellison, D.W. *et al.* Definition of disease-risk stratification groups in childhood medulloblastoma using combined clinical, pathologic, and molecular variables. *J Clin Oncol* **29**, 1400-7 (2011).
17. Brown, H.G. *et al.* "Large cell/anaplastic" medulloblastomas: a Pediatric Oncology Group Study. *J Neuropathol Exp Neurol* **59**, 857-65 (2000).

18. Giangaspero, F. *et al.* Large-cell medulloblastomas. A distinct variant with highly aggressive behavior. *Am J Surg Pathol* **16**, 687-93 (1992).
19. Giangaspero, F. *et al.* Medulloblastoma with extensive nodularity: a variant with favorable prognosis. *J Neurosurg* **91**, 971-7 (1999).
20. Werbowetski-Ogilvie, T.E. From sorting to sequencing in the molecular era: the evolution of the cancer stem cell model in medulloblastoma. *FEBS J* (2021).
21. Batlle, E. & Clevers, H. Cancer stem cells revisited. *Nat Med* **23**, 1124-1134 (2017).
22. Louis, D.N. *et al.* The 2021 WHO Classification of Tumors of the Central Nervous System: a summary. *Neuro Oncol* (2021).
23. Northcott, P.A. *et al.* Medulloblastoma comprises four distinct molecular variants. *J Clin Oncol* **29**, 1408-14 (2011).
24. Cavalli, F.M.G. *et al.* Intertumoral Heterogeneity within Medulloblastoma Subgroups. *Cancer Cell* **31**, 737-754 e6 (2017).
25. Schwalbe, E.C. *et al.* Novel molecular subgroups for clinical classification and outcome prediction in childhood medulloblastoma: a cohort study. *Lancet Oncol* **18**, 958-971 (2017).
26. Northcott, P.A. *et al.* The whole-genome landscape of medulloblastoma subtypes. *Nature* **547**, 311-317 (2017).
27. Gajjar, A. *et al.* Outcomes by Clinical and Molecular Features in Children With Medulloblastoma Treated With Risk-Adapted Therapy: Results of an International Phase III Trial (SJMB03). *J Clin Oncol*, JCO2001372 (2021).
28. McMahon, A.P., Joyner, A.L., Bradley, A. & McMahon, J.A. The midbrain-hindbrain phenotype of Wnt-1-/Wnt-1-mice results from stepwise deletion of engrailed-expressing cells by 9.5 days postcoitum. . *Cell* **69**, 581-595 (1992).
29. Ikeya, M., Lee, S.M., Johnson, J.E., McMahon, A.P. & Takada, S. Wnt signalling required for expansion of neural crest and CNS progenitors. *Nature* **389**, 966-70 (1997).
30. Lie, D.C. *et al.* Wnt signalling regulates adult hippocampal neurogenesis. *Nature* **437**, 1370-5 (2005).
31. Yu, J. & Virshup, David M. Updating the Wnt pathways. *Bioscience Reports* **34**, e00142 (2014).
32. Niehrs, C. The complex world of WNT receptor signalling. *Nat Rev Mol Cell Biol* **13**, 767-779 (2012).
33. Wu, D. & Pan, W. GSK3: a multifaceted kinase in Wnt signaling. *Trends Biochem Sci* **35**, 161-8 (2010).
34. He, T.C. *et al.* Identification of c-MYC as a target of the APC pathway. *Science* **281**, 1509-1512 (1998).
35. Chenn, A. Wnt/beta-catenin signaling in cerebral cortical development. *Organogenesis* **4**, 76-80 (2008).
36. Baeza, N., Masuoka, J., Kleihues, P. & Ohgaki, H. AXIN1 mutations but not deletions in cerebellar medulloblastomas. *Oncogene* **22**, 632 (2003).
37. EBERHART, C.G., TIHAN, T. & BURGER, P.C. Nuclear Localization and Mutation of β-Catenin in Medulloblastomas. *Journal of Neuropathology & Experimental Neurology* **59**, 333-337 (2000).
38. Huang, H. *et al.* APC mutations in sporadic medulloblastomas. *American Journal of Pathology* **156**, 433-7 (2000).

39. Koch, A. *et al.* Somatic mutations of WNT/wingless signaling pathway components in primitive neuroectodermal tumors. *International Journal of Cancer* **93**, 445-449 (2001).
40. Zurawel, R.H., Chiappa, S.A., Allen, C. & Raffel, C. Sporadic Medulloblastomas Contain Oncogenic β-Catenin Mutations. *Cancer Research* **58**, 896-899 (1998).
41. Gibson, P. *et al.* Subtypes of medulloblastoma have distinct developmental origins. *Nature* **468**, 1095-9 (2010).
42. Phoenix, T.N. *et al.* Medulloblastoma Genotype Dictates Blood Brain Barrier Phenotype. *Cancer Cell* **29**, 508-522 (2016).
43. Northcott, P.A. *et al.* Subgroup-specific structural variation across 1,000 medulloblastoma genomes. *Nature* **488**, 49-56 (2012).
44. Nobre, L. *et al.* Pattern of Relapse and Treatment Response in WNT-Activated Medulloblastoma. *Cell Rep Med* **1**(2020).
45. Takebe, N. *et al.* Targeting Notch, Hedgehog, and Wnt pathways in cancer stem cells: clinical update. *Nat Rev Clin Oncol* **12**, 445-64 (2015).
46. Baryawno, N. *et al.* Small-molecule inhibitors of phosphatidylinositol 3-kinase/Akt signaling inhibit Wnt/beta-catenin pathway cross-talk and suppress medulloblastoma growth. *Cancer Res* **70**, 266-76 (2010).
47. Kool, M. *et al.* Molecular subgroups of medulloblastoma: an international meta-analysis of transcriptome, genetic aberrations, and clinical data of WNT, SHH, Group 3, and Group 4 medulloblastomas. *Acta Neuropathol* **123**, 473-84.
48. Kawauchi, D. *et al.* A Mouse Model of the Most Aggressive Subgroup of Human Medulloblastoma. *Cancer Cell* **21**, 168-180 (2012).
49. Pei, Y. *et al.* An animal model of MYC-driven medulloblastoma. *Cancer Cell* **21**, 155-67 (2012).
50. Eberhart, C.G. Three Down and One To Go: Modeling Medulloblastoma Subgroups. *Cancer Cell* **21**, 137-138 (2012).
51. Lin, C.Y. *et al.* Active medulloblastoma enhancers reveal subgroup-specific cellular origins. *Nature* **530**, 57-62 (2016).
52. Hovestadt, V. *et al.* Resolving medulloblastoma cellular architecture by single-cell genomics. *Nature* **572**, 74-79 (2019).
53. Jones, D.T. *et al.* Dissecting the genomic complexity underlying medulloblastoma. *Nature* **488**, 100-5 (2012).
54. Kaur, R. *et al.* OTX2 exhibits cell-context-dependent effects on cellular and molecular properties of human embryonic neural precursors and medulloblastoma cells. *Dis Model Mech* **8**, 1295-309 (2015).
55. Stromecki, M. *et al.* Characterization of a novel OTX2-driven stem cell program in Group 3 and Group 4 medulloblastoma. *Mol Oncol* **12**, 495-513 (2018).
56. Lu, Y. *et al.* OTX2 expression contributes to proliferation and progression in Myc-amplified medulloblastoma. *Am J Cancer Res* **7**, 647-656 (2017).
57. Zagozewski, J. *et al.* An OTX2-PAX3 signaling axis regulates Group 3 medulloblastoma cell fate. *Nat Commun* **11**, 3627 (2020).
58. Morfouace, M. *et al.* Pemetrexed and gemcitabine as combination therapy for the treatment of Group3 medulloblastoma. *Cancer Cell* **25**, 516-29 (2014).
59. Bai, R. *et al.* Evaluation of retinoic acid therapy for OTX2-positive medulloblastomas. *Neuro Oncol* **12**, 655-63 (2010).

60. Freemantle, S.J., Spinella, M.J. & Dmitrovsky, E. Retinoids in cancer therapy and chemoprevention: promise meets resistance. *Oncogene* **22**, 7305-15 (2003).
61. Fu, Y.S. *et al.* CRABP-II methylation: a critical determinant of retinoic acid resistance of medulloblastoma cells. *Mol Oncol* **6**, 48-61 (2012).
62. Zhukova, N. *et al.* Subgroup-specific prognostic implications of TP53 mutation in medulloblastoma. *J Clin Oncol* **31**, 2927-35 (2013).
63. Ramaswamy, V. *et al.* Medulloblastoma subgroup-specific outcomes in irradiated children: who are the true high-risk patients? *Neuro Oncol* **18**, 291-7 (2016).
64. Robinson, G.W. *et al.* Risk-adapted therapy for young children with medulloblastoma (SJYC07): therapeutic and molecular outcomes from a multicentre, phase 2 trial. *Lancet Oncol* **19**, 768-784 (2018).
65. Garcia-Lopez, J., Kumar, R., Smith, K.S. & Northcott, P.A. Deconstructing Sonic Hedgehog Medulloblastoma: Molecular Subtypes, Drivers, and Beyond. *Trends Genet* **37**, 235-250 (2021).
66. Kool, M. *et al.* Genome sequencing of SHH medulloblastoma predicts genotype-related response to smoothened inhibition. *Cancer Cell* **25**, 393-405 (2014).
67. Pugh, T.J. *et al.* Medulloblastoma exome sequencing uncovers subtype-specific somatic mutations. *Nature* **488**, 106-10 (2012).
68. John, A.M. & Schwartz, R.A. Basal Cell Nevus Syndrome: An Update on Genetics and Treatment. *British Journal of Dermatology*, n/a-n/a (2015).
69. Dahmane, N. & Ruiz-i-Altaba, A. Sonic hedgehog regulates the growth and patterning of the cerebellum. *Development* **126**, 3089-3100 (1999).
70. Wallace, V.A. Purkinje-cell-derived Sonic hedgehog regulates granule neuron precursor cell proliferation in the developing mouse cerebellum. *Current Biology* **9**, 445-448 (1999).
71. Wechsler-Reya, R.J. & Scott, M.P. Control of Neuronal Precursor Proliferation in the Cerebellum by Sonic Hedgehog. *Neuron* **22**, 103-114 (1999).
72. Briscoe, J. & Therond, P.P. The mechanisms of Hedgehog signalling and its roles in development and disease. *Nat Rev Mol Cell Biol* **14**, 416-429 (2013).
73. Taipale, J., Cooper, M.K., Maiti, T. & Beachy, P.A. Patched acts catalytically to suppress the activity of Smoothened. *Nature* **418**, 892-896 (2002).
74. Svärd, J. *et al.* Genetic Elimination of Suppressor of Fused Reveals an Essential Repressor Function in the Mammalian Hedgehog Signaling Pathway. *Developmental Cell* **10**, 187-197 (2006).
75. Han, Y.G. *et al.* Dual and opposing roles of primary cilia in medulloblastoma development. *Nat Med* **15**, 1062-5 (2009).
76. Chang, C.H. *et al.* Atoh1 Controls Primary Cilia Formation to Allow for SHH-Triggered Granule Neuron Progenitor Proliferation. *Dev Cell* **48**, 184-199 e5 (2019).
77. Aguilar, A. *et al.* Analysis of human samples reveals impaired SHH-dependent cerebellar development in Joubert syndrome/Meckel syndrome. *Proc Natl Acad Sci U S A* **109**, 16951-6 (2012).
78. Kool, M. *et al.* Molecular subgroups of medulloblastoma: an international meta-analysis of transcriptome, genetic aberrations, and clinical data of WNT, SHH, Group 3, and Group 4 medulloblastomas. *Acta Neuropathol* **123**, 473-84 (2012).
79. Rutkowski, S. *et al.* Treatment of Early Childhood Medulloblastoma by Postoperative Chemotherapy Alone. *New England Journal of Medicine* **352**, 978-986 (2005).

80. Fang, Z. *et al.* Case Report : Li-Fraumeni Syndrome with Central Nervous System Tumors in Two Siblings. *BMC Pediatr* **21**, 588 (2021).
81. Schuller, U. *et al.* Acquisition of granule neuron precursor identity is a critical determinant of progenitor cell competence to form Shh-induced medulloblastoma. *Cancer Cell* **14**, 123-34 (2008).
82. Yang, Z.J. *et al.* Medulloblastoma can be initiated by deletion of Patched in lineage-restricted progenitors or stem cells. *Cancer Cell* **14**, 135-45 (2008).
83. Zhang, L. *et al.* Single-Cell Transcriptomics in Medulloblastoma Reveals Tumor-Initiating Progenitors and Oncogenic Cascades during Tumorigenesis and Relapse. *Cancer Cell* **36**, 302-318 e7 (2019).
84. Lindsey, J.C. *et al.* TERT promoter mutation and aberrant hypermethylation are associated with elevated expression in medulloblastoma and characterise the majority of non-infant SHH subgroup tumours. *Acta Neuropathol* **127**, 307-9 (2014).
85. Remke, M. *et al.* TERT promoter mutations are highly recurrent in SHH subgroup medulloblastoma. *Acta Neuropathol* **126**, 917-29 (2013).
86. Koelsche, C. *et al.* Distribution of TERT promoter mutations in pediatric and adult tumors of the nervous system. *Acta Neuropathol* **126**, 907-15 (2013).
87. Jacobsen, P.F., Jenkyn, D.J. & Papadimitriou, J.M. Establishment of a human medulloblastoma cell line and its heterotransplantation into nude mice. *J Neuropathol Exp Neurol* **44**, 472-85 (1985).
88. Pambid, M.R. *et al.* Overcoming resistance to Sonic Hedgehog inhibition by targeting p90 ribosomal S6 kinase in pediatric medulloblastoma. *Pediatr Blood Cancer* **61**, 107-15 (2014).
89. Liang, L. *et al.* Characterization of novel biomarkers in selecting for subtype specific medulloblastoma phenotypes. *Oncotarget* **6**, 38881-900 (2015).
90. Northcott, P.A. *et al.* Rapid, reliable, and reproducible molecular sub-grouping of clinical medulloblastoma samples. *Acta Neuropathol* **123**, 615-26 (2012).
91. Johnson, S., Chen, H. & Lo, P.K. In vitro Tumorsphere Formation Assays. *Bio Protoc* **3**(2013).
92. Hallahan, A.R. *et al.* The SmoA1 mouse model reveals that notch signaling is critical for the growth and survival of sonic hedgehog-induced medulloblastomas. *Cancer Res* **64**, 7794-800 (2004).
93. Oliver, T.G. *et al.* Loss of patched and disruption of granule cell development in a pre-neoplastic stage of medulloblastoma. *Development* **132**, 2425-39 (2005).
94. Hatton, B.A. *et al.* The Smo/Smo model: hedgehog-induced medulloblastoma with 90% incidence and leptomeningeal spread. *Cancer Res* **68**, 1768-76 (2008).
95. Rusert, J.M. *et al.* Functional precision medicine identifies new therapeutic candidates for medulloblastoma. *Cancer Res* (2020).
96. Genovesi, L.A. *et al.* Patient-derived orthotopic xenograft models of medulloblastoma lack a functional blood-brain barrier. *Neuro Oncol* **23**, 732-742 (2021).
97. Lin, T.L. & Matsui, W. Hedgehog pathway as a drug target: Smoothened inhibitors in development. *Onco Targets Ther* **5**, 47-58 (2012).
98. Taipale, J. *et al.* Effects of oncogenic mutations in Smoothened and Patched can be reversed by cyclopamine. *Nature* **406**, 1005-9 (2000).
99. Berman, D.M. *et al.* Medulloblastoma growth inhibition by hedgehog pathway blockade. *Science* **297**, 1559-61 (2002).

100. Li, Y., Song, Q. & Day, B.W. Phase I and phase II sonidegib and vismodegib clinical trials for the treatment of paediatric and adult MB patients: a systemic review and meta-analysis. *Acta Neuropathol Commun* **7**, 123 (2019).
101. Robinson, G.W. *et al.* Vismodegib Exerts Targeted Efficacy Against Recurrent Sonic Hedgehog-Subgroup Medulloblastoma: Results From Phase II Pediatric Brain Tumor Consortium Studies PBTC-025B and PBTC-032. *J Clin Oncol* **33**, 2646-54 (2015).
102. Gajjar, A. *et al.* Phase I study of vismodegib in children with recurrent or refractory medulloblastoma: a pediatric brain tumor consortium study. *Clin Cancer Res* **19**, 6305-12 (2013).
103. Amakye, D., Jagani, Z. & Dorsch, M. Unraveling the therapeutic potential of the Hedgehog pathway in cancer. *Nat Med* **19**, 1410-22 (2013).
104. Remke, M. *et al.* Adult medulloblastoma comprises three major molecular variants. *J Clin Oncol* **29**, 2717-23 (2011).
105. Morrissy, A.S. *et al.* Divergent clonal selection dominates medulloblastoma at recurrence. *Nature* **529**, 351-7 (2016).
106. Liang, L. *et al.* CD271(+) Cells Are Diagnostic and Prognostic and Exhibit Elevated MAPK Activity in SHH Medulloblastoma. *Cancer Res* **78**, 4745-4759 (2018).
107. Liang, L. *et al.* Characterization of novel biomarkers in selecting for subtype specific medulloblastoma phenotypes. *Oncotarget* (2015).
108. Wu, P.K. & Park, J.I. MEK1/2 Inhibitors: Molecular Activity and Resistance Mechanisms. *Semin Oncol* **42**, 849-62 (2015).
109. Dombi, E. *et al.* Activity of Selumetinib in Neurofibromatosis Type 1-Related Plexiform Neurofibromas. *N Engl J Med* **375**, 2550-2560 (2016).
110. Gross, A., Bishop, R. & Widemann, B.C. Selumetinib in Plexiform Neurofibromas. *N Engl J Med* **376**, 1195 (2017).
111. Banerjee, A. *et al.* A phase I trial of the MEK inhibitor selumetinib (AZD6244) in pediatric patients with recurrent or refractory low-grade glioma: a Pediatric Brain Tumor Consortium (PBTC) study. *Neuro Oncol* **19**, 1135-1144 (2017).
112. Fangusaro, J. *et al.* Selumetinib in paediatric patients with BRAF-aberrant or neurofibromatosis type 1-associated recurrent, refractory, or progressive low-grade glioma: a multicentre, phase 2 trial. *Lancet Oncol* **20**, 1011-1022 (2019).
113. Zhao, X. *et al.* RAS/MAPK Activation Drives Resistance to Smo Inhibition, Metastasis, and Tumor Evolution in Shh Pathway-Dependent Tumors. *Cancer Res* **75**, 3623-35 (2015).
114. Jamie Zagozewski, S.B., Brent J. Guppy, Ludivine Coudière-Morrison, Ghazaleh M. Shahriary, Victor Gordon, Lisa Liang, Stephen Cheng, Christopher J. Porter, Rhonda Kelley, Cynthia Hawkins, Jennifer A. Chan, Yan Liang, Jingjing Gong, Carolina Nör, Olivier Saulnier, Robert J. Wechsler-Reya, Vijay Ramaswamy, Tamra E. Werbowetski-Ogilvie. Combined MEK and JAK/STAT3 pathway inhibition effectively decreases SHH medulloblastoma tumor progression. *Communications Biology* (2022).
115. Perreault, S. *et al.* A phase 2 study of trametinib for patients with pediatric glioma or plexiform neurofibroma with refractory tumor and activation of the MAPK/ERK pathway: TRAM-01. *BMC Cancer* **19**, 1250 (2019).
116. Bouffet, E. *et al.* Trametinib therapy in pediatric patients with low-grade gliomas (LGG) with BRAF gene fusion;a disease specific cohort in the first pediatric testing of trametinib. *Neuro-Oncology* **20**, i114 (2018).

117. Manoharan, N. *et al.* Trametinib for the treatment of recurrent/progressive pediatric low-grade glioma. *J Neurooncol* **149**, 253-262 (2020).
118. Selt, F. *et al.* Response to trametinib treatment in progressive pediatric low-grade glioma patients. *J Neurooncol* (2020).
119. Markowitz, D. *et al.* Pharmacological Inhibition of the Protein Kinase MRK/ZAK Radiosensitizes Medulloblastoma. *Mol Cancer Ther* **15**, 1799-808 (2016).
120. Werbowetski-Ogilvie, T.E., Morrison, L.C., Fiebig-Comyn, A. & Bhatia, M. In vivo generation of neural tumors from neoplastic pluripotent stem cells models early human pediatric brain tumor formation. *Stem Cells* **30**, 392-404 (2012).
121. Morrison, L.C. *et al.* Deconstruction of medulloblastoma cellular heterogeneity reveals differences between the most highly invasive and self-renewing phenotypes. *Neoplasia* **15**, 384-98 (2013).
122. Milde, T. *et al.* HD-MB03 is a novel Group 3 medulloblastoma model demonstrating sensitivity to histone deacetylase inhibitor treatment. *J Neurooncol* **110**, 335-48 (2012).
123. Cancer, M. *et al.* Humanized Stem Cell Models of Pediatric Medulloblastoma Reveal an Oct4/mTOR Axis that Promotes Malignancy. *Cell Stem Cell* **25**, 855-870 e11 (2019).
124. Patro, R., Duggal, G., Love, M.I., Irizarry, R.A. & Kingsford, C. Salmon provides fast and bias-aware quantification of transcript expression. *Nat Methods* **14**, 417-419 (2017).
125. Reimand, J. *et al.* Pathway enrichment analysis and visualization of omics data using g:Profiler, GSEA, Cytoscape and EnrichmentMap. *Nat Protoc* **14**, 482-517 (2019).
126. Lee, J. *et al.* Tumor stem cells derived from glioblastomas cultured in bFGF and EGF more closely mirror the phenotype and genotype of primary tumors than do serum-cultured cell lines. *Cancer Cell* **9**, 391-403 (2006).
127. Gao, M., Yang, J., Gong, H., Lin, Y. & Liu, J. Trametinib Inhibits the Growth and Aerobic Glycolysis of Glioma Cells by Targeting the PKM2/c-Myc Axis. *Front Pharmacol* **12**, 760055 (2021).
128. Malik, S.C. *et al.* In vivo functions of p75(NTR): challenges and opportunities for an emerging therapeutic target. *Trends Pharmacol Sci* **42**, 772-788 (2021).